Journal of Computational and Applied Mathematics 36 (1991) 29–63
North-Holland

Solution of elastic scattering problems in linear acoustics using *h-p* boundary element methods *

L. Demkowicz, J.T. Oden, M. Ainsworth [1] and P. Geng

The Texas Institute for Computational Mechanics, The University of Texas at Austin, Austin, TX 78712, United States

Received 1 October 1990

Abstract

Demkowicz, L., J.T. Oden, M. Ainsworth and P. Geng, Solution of elastic scattering problems in linear acoustics using *h-p* boundary element methods, Journal of Computational and Applied Mathematics 36 (1991) 29–63.

A simplified model problem reduced from the general class of elastic scattering problems is analyzed. Both classical Helmholtz and hypersingular formulations are discussed and a general *h-p* boundary element method based on the Burton–Miller combination of both approaches is formulated. A simple L^2-residual a posteriori error estimate is discussed as a basis of adaptive *h*- or *p*-refinements.

Keywords: Acoustics, scattering, boundary element methods, error estimates, adaptive methods.

1. Introduction. Elastic scattering problems, a simplified model problem

The problems of scattering by an elastic structure submerged in a fluid, acoustical medium have long been subjects of both fundamental-theoretical and practical investigations (see, e.g., [11,12]). Recently, in [7], a new practical approach has been proposed, coupling finite elements to resolve the elastic structure with the classical Helmholtz boundary integral formulation for the acoustical fluid. In this paper we report some initial investigations pursuing essentially the same idea, directed (eventually) at a development of fully automatic, self-adaptive, *h-p* adaptive strategies to resolve the problem.

The idea of applying adaptive finite (boundary) element methods, including *h-p* methods delivering exponential rates of convergence, to boundary integral equations is not new and has been intensively studied recently (see, e.g., [3,20–23,28,29,32]). However, for both rigid and elastic scattering problems for a full range of wave numbers, several complications add to the complexity of this particular problem.

* This work was supported by the Office of Naval Research under Contract N00014-89-J-1451.

[1] On leave from Mathematics Department, Lancaster University, Lancaster, United Kingdom LA1 4YF.

0377-0427/91/$03.50 © 1991 – Elsevier Science Publishers B.V. (North-Holland)

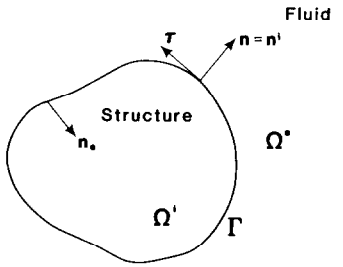

Fig. 1. Formulation of the fluid–structure interaction problem.

The first is that of forbidden frequencies. For some wave numbers, the classical Helmholtz formulation breaks down (becomes singular) and has to be modified. Several solutions to the problem have been proposed, including the use of modified Green's functions (see, e.g., [8,24,30]) or the Burton–Miller approach [4], which we follow in this paper. For these classes of problems, special difficulties exist in deriving a posteriori error estimates and in developing adaptive strategies to cope with the multiple boundary integral formulations of the same problem. This issue is also addressed in this work.

The plan of the presentation is as follows: we conclude this introduction with a formulation of a simplified model problem which is to be the subject of this paper. In Section 2, the classical Helmholtz and hypersingular formulations are discussed and, in Section 3, the numerical solution of these equations is addressed. Section 4 presents some simple experiments. The issue of error estimation and adaptive h- and p-refinement is taken up in Section 5 and some elementary analyses of the a posteriori error estimation scheme are given in Section 6. We conclude with some illustrative numerical experiments in Section 7.

Formulation of the problem

Restricting ourselves, for simplicity, to two-dimensional simulations, we formulate the problem as follows (see Fig. 1). Given a closed curve Γ, we consider the interior domain Ω^{i} and the exterior domain Ω^{e} and wish to determine:

- the displacement field $\boldsymbol{u}(\boldsymbol{x}, t)$ of an elastic structure occupying the interior domain, i.e., $\boldsymbol{x} \in \Omega^{\mathrm{i}} \cup \Gamma$;
- the total velocity $\boldsymbol{v}(\boldsymbol{x}, t)$ and pressure $p(\boldsymbol{x}, t)$ of an acoustical medium occupying the exterior domain, i.e., $\boldsymbol{x} \in \Omega^{\mathrm{e}} \cup \Gamma$, where

$$\boldsymbol{v} = \boldsymbol{v}^{\mathrm{inc}} + \boldsymbol{v}^{\mathrm{s}}, \qquad p = p^{\mathrm{inc}} + p^{\mathrm{s}}, \tag{1.1}$$

with $\boldsymbol{v}^{\mathrm{inc}}$ and p^{inc} (given) the incident velocity and pressure fields defined on the whole plane $\mathbb{R}^2$ and $\boldsymbol{v}^{\mathrm{s}}$ and p^{s} the *unknown* scattered velocity and pressure fields defined in the exterior domain, respectively.

Equations to be satisfied include:

- equations of motion for the linear, elastic body,

$$\rho_{\mathrm{s}} u_{k,tt} - (E_{klrs}\epsilon_{rs})_{,l} = 0 \quad \text{in } \Omega^{\mathrm{i}}, \tag{1.2}$$

where ρ_{s} is the density of the solid, E_{klrs} denotes the elasticities satisfying the customary ellipticity and symmetry assumptions, and

$$\epsilon_{rs} = \tfrac{1}{2}(u_{r,s} + u_{s,r}) \tag{1.3}$$

denotes the strain tensor. As usual, the commas indicate the differentiation with respect to time $(\cdot)_{,t}$ or space $(\cdot)_{,i}$ variables;

- equations of linear acoustics,

$$\left.\begin{aligned} p_{,t} + \rho_f c^2 v_{j,j} &= 0 \\ v_{j,t} + \frac{1}{\rho_f} p_{,j} &= 0 \end{aligned}\right\} \quad \text{in } \Omega^e, \tag{1.4}$$

where ρ_f is the density of the fluid and c denotes the sound speed;

- compatibility conditions on the boundary Γ,

$$\left.\begin{aligned} u_{n,t} &= -v_n \\ \sigma_n(\boldsymbol{u}) &= -p \\ \sigma_\tau(\boldsymbol{u}) &= 0 \end{aligned}\right\} \quad \text{on } \Gamma, \tag{1.5}$$

where

$$u_n = u_k n_k^i, \qquad v_n = v_k n_k^e \tag{1.6}$$

denote the normal displacement and velocity, respectively, ($\boldsymbol{n}^i$ and $\boldsymbol{n}^e$ stand for the *outward* normal unit vectors for the interior and exterior domains, respectively, see Fig. 1), and $\sigma_n(\boldsymbol{u})$ and $\sigma_\tau(\boldsymbol{u})$ stand for the normal and tangential components of the stress vector corresponding to the displacement $\boldsymbol{u}$,

$$\sigma_n(\boldsymbol{u}) = E_{klrs}\epsilon_{rs}(\boldsymbol{u}) n_l^i n_k^i, \qquad \sigma_\tau(\boldsymbol{u}) = E_{klrs}\epsilon_{rs}(\boldsymbol{u}) n_l^i \tau_k, \tag{1.7}$$

with $\boldsymbol{\tau} = (\tau_k)$ the tangential unit vector (compare Fig. 1)

$$\tau_1 = -n_2^i, \qquad \tau_2 = n_1^i; \tag{1.8}$$

- conditions at "infinity",

$$\boldsymbol{v}^s, \; p^s = 0 \tag{1.9}$$

in the sense of the Sommerfeld radiation condition.

Elimination of the acoustic velocity vector leads to the wave equation replacing the equations of acoustics

$$p_{,tt} - c^2 p_{,jj} = 0, \tag{1.10}$$

and the first of the compatibility conditions replaced by

$$u_{n,tt} = \frac{1}{\rho_f} \frac{\partial p}{\partial n_e}. \tag{1.11}$$

Finally, assuming the harmonic time variation,

$$p^{inc}(\boldsymbol{x}, t) = e^{i\omega t} p^{inc}(\boldsymbol{x}), \qquad p^s(\boldsymbol{x}, t) = e^{i\omega t} p^s(\boldsymbol{x}), \qquad \boldsymbol{u}(\boldsymbol{x}, t) = e^{i\omega t}\boldsymbol{u}(\boldsymbol{x}), \tag{1.12}$$

we obtain the following boundary value problem:

$$\left.\begin{aligned}
&\text{Find } \boldsymbol{u} = \boldsymbol{u}(\boldsymbol{x}),\ p = p(\boldsymbol{x}) \text{ such that} \\
&\rho_s \omega^2 u_k + \left(E_{klrs}\epsilon_{rs}(\boldsymbol{u})\right)_{,l} = 0 \quad \text{in } \Omega^i, \\
&k^2 p + p_{,jj} = 0 \quad \text{in } \Omega^e, \\
&\left.\begin{aligned}
&\rho_f \omega^2 u_n = -\frac{\partial p}{\partial n_e} \\
&\sigma_n(\boldsymbol{u}) = -p \\
&\sigma_\tau(\boldsymbol{u}) = 0
\end{aligned}\right\} \quad \text{on } \Gamma, \\
&\text{plus the Sommerfeld condition at } \infty.
\end{aligned}\right\} \tag{1.13}$$

Here $\boldsymbol{u}(\boldsymbol{x})$ and $p(\boldsymbol{x})$ are the spatial variations of the displacement vector and pressure in (1.12), respectively, and $k = \omega/c$ is the wave number.

In this paper we focus our attention on a further simplified problem, replacing the linear elasticity model with a "spring-like" relation

$$\sigma_n(\boldsymbol{u}) = -Eu_n. \tag{1.14}$$

This leads simply to the Helmholtz equation for the pressure,

$$-\Delta p - k^2 p = 0 \quad \text{in } \Omega^e, \tag{1.15}$$

accompanied by the Cauchy boundary condition

$$\frac{\partial p}{\partial n_e} + \epsilon p = 0 \quad \text{on } \Gamma, \tag{1.16}$$

and the Sommerfeld condition at infinity. Here Δ stands for the Laplace operator and

$$\epsilon = \rho_f \frac{\omega^2}{E}. \tag{1.17}$$

In the case of rigid scattering, $\epsilon = 0$ and the problem reduces to the exterior Neumann problem for the Helmholtz equation.

2. Boundary integral (BI) formulations

In this section we show how the problem (1.15), (1.16) may be formulated as an integral equation. The integral equation formulation is not unique and alternative schemes offer various advantages and disadvantages both theoretically and numerically. We shall derive both the classical boundary Helmholtz and the hypersingular integral equations. The derivations are standard (see, e.g., [14,17]) but we shall repeat the arguments since it will serve to introduce the various types of integrals and notations used, in addition to keeping the current work self-contained.

Helmholtz integral equation

We begin by recalling that the 2-D fundamental solution of the Helmholtz equation (1.15) is:

$$\Phi(x, y) = \tfrac{1}{4} i H_0^{(1)}(kr), \quad r \neq 0, \tag{2.1}$$

where k is the wavenumber, $i^2 = -1$ and $r = \| x - y \|$. The function $H_0^{(1)}(z)$ is the zeroth-order Hankel function of the first kind. We may decompose $\Phi(x, y)$ as

$$\Phi(x, y) = \frac{1}{2\pi} J_0(kr) \log \frac{1}{r} + \phi(kr), \tag{2.2}$$

where $\phi \in C^\infty(\mathbb{R})$ and J_0 is the Bessel function of the first kind:

$$J_0(z) = \sum_{k=0}^{\infty} \frac{(-1)^k}{(k!)^2} \left(\tfrac{1}{2} z\right)^{2k}. \tag{2.3}$$

Together, (2.2) and (2.3) show that the singular behavior of $\Phi(x, y)$ as $r \to 0$ is the same as the fundamental solution of Laplace's equation:

$$\Phi(x, y) = \frac{1}{2\pi} \log \frac{1}{r} + \Phi_0(r), \tag{2.4}$$

where Φ_0 is a regular contribution.

Let $u = u(y)$ denote a classical solution of the model problem (1.15), (1.16) along with the Sommerfeld radiation condition at infinity. The typical assumption regarding the regularity of u is $u \in C^2(\Omega) \cap C^{1,\alpha}(\bar{\Omega})$, where $C^{1,\alpha}(\bar{\Omega})$ is the space of functions whose first derivatives are Hölder continuous with exponent $\alpha \in (0, 1)$.

Firstly, let $x \in \Omega^e$ be such that the ball

$$B_\epsilon(x) = \{ y \in \mathbb{R}^2 : \| x - y \| \leqslant \epsilon \} \tag{2.5}$$

is completely contained in Ω^e for some sufficiently small $\epsilon > 0$ (see Fig. 2). The surface of this ball is denoted by $S_\epsilon(x)$:

$$S_\epsilon(x) = \{ y \in \mathbb{R}^2 : \| x - y \| = \epsilon \}. \tag{2.6}$$

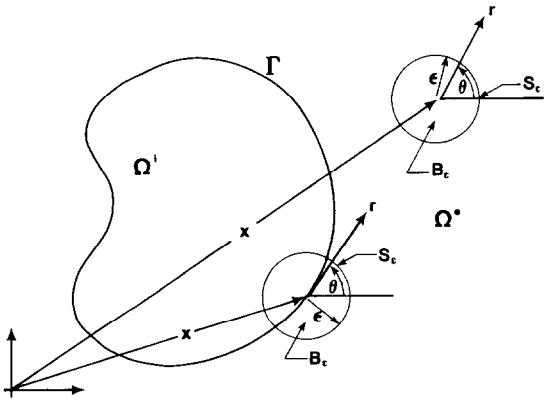

Fig. 2. Derivation of the boundary integral equations.

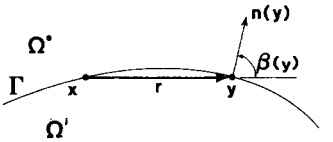

Fig. 3. Definition of $\beta(y)$.

Applying Green's second theorem to the functions $u(\cdot)$ and $\Phi(x, \cdot)$ in the domain $\Omega^e \setminus B_\epsilon(x)$ gives

$$\begin{aligned}
&\int_{\Omega^e \setminus B_\epsilon(x)} \{u(y)\Delta_y \Phi(x,y) - \Delta u(y)\Phi(x,y)\}\, dy \\
&= \int_\Gamma \left\{ u(y) \frac{\partial \Phi}{\partial n_e(y)}(x,y) - \frac{\partial u}{\partial n_e(y)}(y)\Phi(x,y) \right\} ds(y) \\
&\quad + \int_{S_\epsilon(x)} \left\{ u(y) \frac{\partial \Phi}{\partial n_e(y)}(x,y) - \frac{\partial u}{\partial n_e(y)}(y)\Phi(x,y) \right\} ds(y),
\end{aligned} \tag{2.7}$$

where $n_e(y)$ denotes the unit outward normal vector for the domain $\Omega^e \setminus B_\epsilon(x)$. Notice in particular that $n_e(y)$ is directed towards the center of the domain $B_\epsilon(x)$. In deriving (2.7) we have omitted the integral over the surface at infinity since it vanishes due to the Sommerfeld conditions. The volume integral in (2.7) vanishes since both $u(\cdot)$ and $\Phi(x, \cdot)$ satisfy the Helmholtz equation in the domain $\Omega^e \setminus B_\epsilon(x)$.

From (2.4) we have for $y \in S_\epsilon(x)$,

$$\frac{\partial \Phi}{\partial n_e(y)}(x,y) = \frac{1}{2\pi r} - \Phi_0'(r), \tag{2.8}$$

since $\boldsymbol{n}_e(y)$ points in the opposite direction of $\boldsymbol{r}$. Therefore,

$$\begin{aligned}
&\left| u(x) - \int_{S_\epsilon(x)} u(y) \frac{\partial \Phi}{\partial n_e(y)}(x,y)\, ds(y) \right| \\
&= \left| u(x) - \int_{S_\epsilon(x)} u(y) \left(\frac{1}{2\pi\epsilon} - \Phi_0'(\epsilon) \right) ds(y) \right| \\
&\leqslant \left| u(x) - \frac{1}{2\pi\epsilon} \int_{S_\epsilon(x)} u(y)\, ds(y) \right| + 2\pi\epsilon \max_{y \in \Omega^e} |u(y)|\, |\Phi_0'(\epsilon)| \to 0 \quad \text{as } \epsilon \to 0,
\end{aligned} \tag{2.9}$$

where we have applied the mean value theorem to the first term, whilst for the second term we used $\Phi_0 \in C^1(\mathbb{R}^2)$ and the uniform boundedness of u. Furthermore, since $u \in C^1(\Omega)$,

$$\begin{aligned}
\left| \int_{S_\epsilon(x)} \frac{\partial u}{\partial n_e(y)}(y)\Phi(x,y)\, ds(y) \right| &\leqslant 2\pi\epsilon \max_{y \in \Omega^e} |\nabla u(y)| \left(\frac{1}{2\pi} \log \frac{1}{\epsilon} + |\Phi_1(\epsilon)| \right) \\
&\to 0 \quad \text{as } \epsilon \to 0.
\end{aligned} \tag{2.10}$$

Combining (2.7)–(2.10) yields the result that for $x \in \Omega^e$,

$$u(x) = \int_\Gamma \left\{ u(y) \frac{\partial \Phi}{\partial n(y)}(x,y) - \frac{\partial u}{\partial n(y)}(y)\Phi(x,y) \right\} ds(y), \tag{2.11}$$

where $n(y) = -n_e(y)$ is the unit outward normal vector for the *interior* domain Ω^i.

The Helmholtz boundary equation can be derived now in two different ways. In the first approach we converge with the point x to the boundary Γ and use the continuity (or discontinuity) properties of the single and double layer potentials present in (2.11) (e.g., [17,

p.68]). In an alternative approach we simply place the point x on Γ right from the very beginning and reproduce the same arguments as in the derivation of (2.11).

Our starting point is the analogue of (2.7):

$$\int_{\Omega^e \setminus B_\epsilon} \left[u(y) \Delta_y \Phi(x, y) - \Delta u(y) \Delta(x, y) \right] \mathrm{d}y$$
$$= \int_{\Gamma \setminus B_\epsilon} \left[u(y) \frac{\partial \Phi}{\partial n_e(y)}(x, y) - \frac{\partial u}{\partial n_e(y)}(y) \Phi(x, y) \right] \mathrm{d}s(y)$$
$$+ \int_{S_\epsilon \cap \Omega^e} \left[u(y) \frac{\partial \Phi}{\partial n_e(y)}(x, y) - \frac{\partial u}{\partial n_e(y)}(y) \Phi(x, y) \right] \mathrm{d}s(y). \tag{2.12}$$

Here, with a slight abuse of notation, we denote $\Gamma \setminus (\Gamma \cap B_\epsilon)$ by $\Gamma \setminus B_\epsilon$. Assuming additionally that the boundary Γ is C^1-continuous, we get for the first part of the second boundary integral

$$\int_{S_\epsilon \cap \Omega^e} u(y) \frac{\partial \Phi}{\partial n_e(y)}(x, y) \, \mathrm{d}s = \int_{\theta_1}^{\theta_2} (u(x) + \mathrm{O}(\epsilon)) \left(\frac{1}{2\pi} \frac{1}{\epsilon} - \Phi_0'(\epsilon) \right) \epsilon \, \mathrm{d}\theta \to \tfrac{1}{2} u(x) \tag{2.13}$$

as $\epsilon \to 0$, since for the C^1-boundary

$$\theta_2 - \theta_1 \to \pi. \tag{2.14}$$

The second part, as before, converges to 0.

Passing to the limit with $\epsilon \to 0$ in the first boundary integral in (2.12), we interpret it in the Cauchy principal value (CPV) sense, i.e.,

$$⨍_\Gamma \left[u(y) \frac{\partial \Phi}{\partial n_e(y)}(x, y) - \frac{\partial u}{\partial n_e(y)}(y) \Phi(x, y) \right] \mathrm{d}s(y) = \lim_{\epsilon \to 0} \int_{\Gamma \setminus B_\epsilon} [\cdot] \, \mathrm{d}s(y). \tag{2.15}$$

However, a closer look at both terms in the integrand reveals that they are (Lebesgue) integrable! Indeed,

$$\frac{\partial \Phi}{\partial n_e(y)}(x, y) = -\frac{\partial \Phi}{\partial n(y)}(x, y) = -\frac{\partial \Phi}{\partial r}(x, y) \frac{\partial r}{\partial n(y)}(x, y)$$
$$= -\frac{\partial \Phi}{\partial r}(x, y) \frac{\boldsymbol{r} \cdot \boldsymbol{n}(y)}{r} = -\frac{\partial \Phi}{\partial r}(x, y) \cos \beta(y)$$
$$= \left(\frac{1}{2\pi} \frac{1}{r} - \Phi_0'(r) \right) \cos \beta(y), \tag{2.16}$$

where $\beta(y)$ is the angle between the relative position vector $\boldsymbol{r} = y - x$ and the normal $\boldsymbol{n}(y)$ (see Fig. 3). As for C^1-boundaries both the distance r and $\cos \beta(y)$ converge to zero at the same rate, the normal derivative (2.16) is not only Lebesgue integrable but continuous at x as well (and therefore bounded on Γ).

The second contribution in (2.15) is only weakly singular, i.e., the integrand is Lebesgue integrable and consequently there is no need for the CPV integral as

$$\lim_{\epsilon \to 0} \int_{\Gamma \setminus B_\epsilon} [\cdot] \, \mathrm{d}s(y) = \int_\Gamma [\cdot] \, \mathrm{d}s(y). \tag{2.17}$$

Thus, we have arrived at the classical Helmholtz boundary integral equation in the form

$$\tfrac{1}{2}u(x) = \int_\Gamma \left[u(y) \frac{\partial \Phi}{\partial n(y)}(x, y) - \frac{\partial u}{\partial n(y)}(y) \Phi(x, y) \right] ds(y), \quad x \in \Gamma, \tag{2.18}$$

where

$$\Phi(x, y) = \Phi(r) = \frac{1}{2\pi} \ln\left(\frac{1}{r}\right) + \Phi_0(r),$$
$$\frac{\partial \Phi}{\partial n(y)} = \left(-\frac{1}{2\pi} \frac{1}{r} + \Phi_0'(r) \right) \cos \beta(y). \tag{2.19}$$

Hypersingular formulation

We begin by selecting a point $\hat{x}$ on boundary Γ. Taking $n(\hat{x})$, the outward unit vector for the interior domain, we differentiate both sides of formula (2.11) in the direction of $n(\hat{x})$ giving

$$\frac{\partial u}{\partial n(\hat{x})}(x) = \int_\Gamma \left[u(y) \frac{\partial^2 \Phi}{\partial n(\hat{x})\, \partial n(y)}(x, y) - \frac{\partial u}{\partial n(y)} \frac{\partial \Phi}{\partial n(\hat{x})}(x, y) \right] ds(y). \tag{2.20}$$

Note the difference between the points x and $\hat{x}$!

Again two different techniques in deriving the hypersingular formulation are possible. In the first approach (see, e.g., [19]) one can pass with $x \to \hat{x}$ in (2.20) and examine carefully the proper sense of the limit. Again, an alternative approach is possible, by placing point x right from the very beginning on boundary Γ. Our starting point is once again the second Green's identity applied to the solution $u(y)$ and, this time, to the derivative

$$\frac{\partial \Phi}{\partial n(x)}(x, y), \quad x \in \Gamma, \tag{2.21}$$

with the point x placed on boundary Γ and the exterior domain modified by subtracting a ball B_ϵ (recall Fig. 2). We have

$$\begin{aligned} &\int_{\Omega^e \setminus B_\epsilon} \left[u(y) \Delta_y \frac{\partial \Phi}{\partial n(x)}(x, y) - \Delta u(y) \frac{\partial \Phi}{\partial n(x)}(x, y) \right] dy \\ &\quad = \int_{\Gamma \setminus B_\epsilon} \left[u(y) \frac{\partial^2 \Phi}{\partial n_e(y)\, \partial n(x)}(x, y) - \frac{\partial u}{\partial n_e(y)}(y) \frac{\partial \Phi}{\partial n(x)}(x, y) \right] ds(y) \\ &\qquad + \int_{S_\epsilon \cap \Omega^e} \left[u(y) \frac{\partial^2 \Phi}{\partial n_e(y)\, \partial n(x)}(x, y) - \frac{\partial u}{\partial n_e(y)}(y) \frac{\partial \Phi}{\partial n(x)}(x, y) \right] ds(y). \end{aligned} \tag{2.22}$$

As before, if u is a solution to the Helmholtz equation, the first integral must vanish.

Next, similar to (2.16) we have

$$\begin{aligned} -\frac{\partial \Phi}{\partial n(x)}(x, y) &= -\frac{\partial \Phi}{\partial r}(x, y) \frac{r \cdot n(x)}{r} = -\frac{\partial \Phi}{\partial r}(x, y) \cos \beta(x) \\ &= \left(\frac{1}{2\pi} \frac{1}{r} - \Phi_0'(r) \right) \cos \beta(x), \end{aligned} \tag{2.23}$$

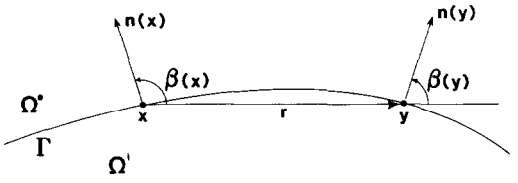

Fig. 4. Definition of angles $\beta(x)$, $\beta(y)$.

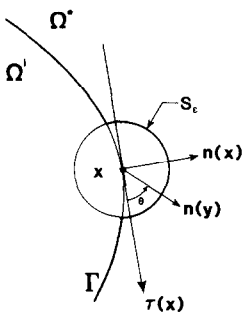

Fig. 5. Derivation of the hypersingular formulation.

where, this time, $\beta(x)$ is the angle between the relative position vector $\boldsymbol{r} = \boldsymbol{y} - \boldsymbol{x}$ and the normal $\boldsymbol{n}(x)$ (see Fig. 4). Differentiating (2.23) we get

$$\frac{\partial^2 \Phi}{\partial n_e(y)\,\partial n(x)}(x, y) = -\frac{\partial^2 \Phi}{\partial n(y)\,\partial n(x)}(x, y) = \frac{\partial}{\partial n(y)}\left[-\frac{\partial \Phi}{\partial r}(x, y)\frac{\boldsymbol{r}\cdot\boldsymbol{n}(x)}{r}\right]$$
$$= -\frac{\partial^2 \Phi}{\partial r^2}(x, y)\frac{\boldsymbol{r}\cdot\boldsymbol{n}(y)}{r}\frac{\boldsymbol{r}\cdot\boldsymbol{n}(x)}{r} - \frac{\partial \Phi}{\partial r}(x, y)\frac{\partial}{\partial n(y)}\left(\frac{\boldsymbol{r}\cdot\boldsymbol{n}(x)}{r}\right) \tag{2.24}$$

But

$$\frac{\partial}{\partial n(y)}\left(\frac{\boldsymbol{r}\cdot\boldsymbol{n}(x)}{r}\right) = \frac{\partial}{\partial n(y)}\left(\frac{1}{r}\right)(\boldsymbol{r}\cdot\boldsymbol{n}(x)) + \frac{1}{r}\frac{\partial}{\partial n(y)}(\boldsymbol{r}\cdot\boldsymbol{n}(x))$$
$$= -\frac{1}{r^2}\frac{\partial r}{\partial n(y)}(x, y)(\boldsymbol{r}\cdot\boldsymbol{n}(x)) + \frac{1}{r}\boldsymbol{n}(y)\cdot\boldsymbol{n}(x)$$
$$= -\frac{1}{r}\cos\beta(x)\cos\beta(y) + \frac{1}{r}\cos\gamma, \tag{2.25}$$

where

$$\cos\gamma = \boldsymbol{n}(y)\cdot\boldsymbol{n}(x), \tag{2.26}$$

and therefore (2.24) leads to

$$\frac{\partial^2 \Phi}{\partial n_e(y)\,\partial n(x)}(x, y)$$
$$= \left[-\frac{\partial^2 \Phi}{\partial r^2}(x, y) + \frac{1}{r}\frac{\partial \Phi}{\partial r}(x, y)\right]\cos\beta(x)\cos\beta(y) - \frac{1}{r}\frac{\partial \Phi}{\partial r}(x, y)\cos\gamma$$
$$= \left[-\frac{1}{2\pi}\frac{1}{r^2} - \Phi_0''(r) + \frac{1}{r}\left(-\frac{1}{2\pi}\frac{1}{r} + \Phi_0'(r)\right)\right]\cos\beta(x)\cos\beta(y)$$
$$+ \frac{1}{r}\left[\frac{1}{2\pi}\frac{1}{r} - \Phi_0'(r)\right]\cos\gamma$$
$$= \left[-\frac{1}{2\pi}\frac{2}{r^2} - \Phi_0''(r) + \frac{1}{r}\Phi_0'(r)\right]\cos\beta(x)\cos\beta(y) + \left[\frac{1}{2\pi}\frac{1}{r^2} - \frac{1}{r}\Phi_0'(r)\right]\cos\gamma. \tag{2.27}$$

Note that the only singular contribution to (2.27) on a C^1-continuous boundary Γ is

$$\frac{1}{2\pi}\frac{1}{r^2}\cos\gamma, \tag{2.28}$$

whereas all the other terms are bounded at x.

We now are ready to investigate the limiting behavior of the second boundary integral in (2.22). For points $y \in S_\epsilon$ (Fig. 5), in the local polar system of coordinates r, θ, centered at x, we have

$$\beta(y)=0, \qquad \beta(x)=\tfrac{1}{2}\pi-\theta, \qquad \gamma=\tfrac{1}{2}\pi-\theta. \tag{2.29}$$

Thus we have (Fig. 5)

$$\begin{aligned}
&\int_{S_\epsilon\cap\Omega^e}\left[u(y)\frac{\partial^2\Phi}{\partial n_e(y)\,\partial n(x)}(x,y)\right]ds(y)\\
&=\int_{\theta_1}^{\theta_2}\left[u(x)+\frac{\partial u}{\partial\tau(x)}(x)\epsilon\cos\theta+\frac{\partial u}{\partial n(x)}(x)\epsilon\sin\theta+O(\epsilon^2)\right]\\
&\quad\times\left[-\frac{1}{2\pi}\frac{2}{\epsilon^2}-\Phi_0''(\epsilon)+\frac{1}{\epsilon}\Phi_0'(\epsilon)+\frac{1}{2\pi}\frac{1}{\epsilon^2}-\frac{1}{\epsilon}\Phi_0'(\epsilon)\right]\epsilon\sin\theta\,d\theta\\
&=\int_{\theta_1}^{\theta_2}\left[u(x)+\frac{\partial u}{\partial\tau(x)}(x)\epsilon\cos\theta+\frac{\partial u}{\partial n(x)}(x)\epsilon\sin\theta+O(\epsilon^2)\right]\\
&\quad\times\left[-\frac{1}{2\pi}\frac{1}{\epsilon^2}-\phi_0''(\epsilon)\right]\epsilon\sin\theta\,d\theta\\
&=-\frac{1}{2\pi\epsilon}u(x)\int_{\theta_1}^{\theta_2}\sin\theta\,d\theta-\frac{1}{2\pi}\frac{\partial u}{\partial\tau}(x)\int_{\theta_1}^{\theta_2}\sin\theta\cos\theta\,d\theta\\
&\quad-\frac{1}{2\pi}\frac{\partial u}{\partial n(x)}(x)\int_{\theta_1}^{\theta_2}\sin^2\theta\,d\theta+O(\epsilon).
\end{aligned} \tag{2.30}$$

For C^1-continuous boundary Γ, as $\epsilon\to 0$, $\theta_2-\theta_1$ converges to π and

- the first term behaves as $-u(x)/(\pi\epsilon)$;
- the second term converges to zero;
- the third term converges to $-\frac{1}{4}\partial u(x)/\partial n(x)$.

By the same reasoning we conclude that the limiting behavior of the second part of the second boundary integral in (2.22)

$$\begin{aligned}
&-\int_{S_\epsilon\cap\Omega^e}\frac{\partial u}{\partial n_e(y)}(y)\frac{\partial\Phi}{\partial n(x)}(x,y)\,ds(y)\\
&=\int_{S_\epsilon\cap\Omega^e}\frac{\partial u}{\partial r}(y)\frac{\partial\Phi}{\partial n(x)}(x,y)\,ds(y)\\
&=\int_{\theta_1}^{\theta_2}\left[\frac{\partial u}{\partial\tau(x)}(x)\cos\theta+\frac{\partial u}{\partial n(x)}(x)\sin\theta+O(\epsilon)\right]\left[-\frac{1}{2\pi}\frac{1}{\epsilon}+\Phi_0'(\epsilon)\right]\epsilon\sin\theta\,d\theta\\
&=\frac{1}{2\pi}\frac{\partial u}{\partial\tau(x)}(x)\int_{\theta_1}^{\theta_2}\cos\theta\sin\theta\,d\theta+\frac{1}{2\pi}\frac{\partial u}{\partial n(x)}(x)\int_{\theta_1}^{\theta_2}\sin^2\theta\,d\theta+O(\epsilon)\\
&\to-\frac{1}{4}\frac{\partial u}{\partial n(x)}(x).
\end{aligned} \tag{2.31}$$

Turning back now to the interpretation of the first boundary integrals in (2.22), we introduce

- the Hadamard finite-part integral defined as

$$\begin{aligned}
&\oint_\Gamma u(y)\frac{\partial^2\Phi}{\partial n_e(y)\,\partial n(x)}(x, y)\,ds(y)\\
&\quad\overset{\text{def}}{=}\lim_{\epsilon\to 0}\left\{\int_{\Gamma\setminus B_\epsilon} u(y)\frac{\partial^2\Phi}{\partial n_e(y)\,\partial n(x)}(x, y)\,ds(y)-\frac{u(x)}{\pi\epsilon}\right\}\\
&\quad=\lim_{\epsilon\to 0}\left\{\int_{\Gamma\setminus B_\epsilon} u(y)\left[\frac{1}{\pi}\frac{1}{r^2}\cos\gamma\right]ds(y)-\frac{u(x)}{\pi\epsilon}\right\}\\
&\qquad+\int_\Gamma u(y)\left\{\left[-\frac{1}{2\pi}\frac{2}{r^2}-\Phi_0''(r)+\frac{1}{r}\Phi_0'(r)\right]\cos\beta(x)\cos\beta(y)\right.\\
&\qquad\qquad\left.+\left[-\frac{1}{r}\Phi_0'(r)\right]\cos\gamma\right\}ds(y);
\end{aligned}\tag{2.32}$$

- the CPV integral

$$\oint\frac{\partial u}{\partial n(y)}(y)\frac{\partial\Phi}{\partial n(x)}(x, y)\,ds(y)\overset{\text{def}}{=}\lim_{\epsilon\to 0}\int_{\Gamma\setminus B_\epsilon}\frac{\partial u}{\partial n(y)}(y)\frac{\partial\Phi}{\partial n(x)}(x, y)\,ds(y).\tag{2.33}$$

However, as in the Helmholtz formulation, the function $\partial\Phi/\partial n(x)$ is Lebesgue integrable (compare (2.23)) and therefore the CPV integral reduces to the usual Lebesgue integral.

Finally, let us note that for a C^1-Hölder continuous solution of the Helmholtz equation, the Hadamard finite-part integral must converge as the left-hand side of (2.22) is zero and the second boundary integral (with the singularity removed) converges.

The operator characterizing the final hypersingular formulation reads as follows:

$$\begin{aligned}
&\frac{1}{2}\frac{\partial u}{\partial n(x)}(x)-\oint_\Gamma u(y)\frac{\partial^2\Phi}{\partial n(x)\,\partial n(y)}(x, y)\,ds(y)+\int_\Gamma\frac{\partial u}{\partial n(y)}(y)\\
&\quad\frac{\partial\Phi}{\partial n(x)}(x, y)\,ds(y)=0.
\end{aligned}\tag{2.34}$$

A summary

Both Helmholtz and hypersingular formulations have been derived so far for *any* function satisfying the Helmholtz equation and the Sommerfeld condition at infinity. Thus they are both applicable only to the scattered pressure field. In order to obtain formulations in terms of the *total pressure*, one has to repeat both derivations for the incident pressure, except that the integration will take place now over the *interior domain* (thus no Sommerfeld condition for the incident pressure is required). This results in a sign change in the final formulas of the form

$$-\tfrac{1}{2}p^{\text{inc}}(x)-\int_\Gamma\left[p^{\text{inc}}(y)\frac{\partial\Phi}{\partial n(y)}(x, y)-\frac{\partial p^{\text{inc}}}{\partial n(y)}(y)\Phi(x, y)\right]ds(y)\tag{2.35}$$

for the Helmholtz formulation, and

$$-\frac{1}{2}\frac{\partial p^{\text{inc}}}{\partial n(x)} + \oint_\Gamma p^{\text{inc}}(y)\frac{\partial^2 \Phi}{\partial n(x)\,\partial n(y)}(x, y)\,ds(y) + \int_\Gamma \frac{\partial p^{\text{inc}}}{\partial n(y)}(y) \times \frac{\partial \Phi}{\partial n(x)}(x, y)\,ds(y). \tag{2.36}$$

Applying (2.35) and (2.36) to the scattered pressure field and summing up (2.18) with (2.35) and (2.34) with (2.36), we obtain the final formulations in the form:

Helmholtz boundary integral formulation

$$\left.\begin{aligned} &\text{Find } p \text{ such that} \\ &\tfrac{1}{2}p(x) - \int_\Gamma p(y)\frac{\partial \Phi}{\partial n(y)}\,ds(y) + \int_\Gamma \frac{\partial p}{\partial n(y)}(y)\Phi(x, y)\,ds(y) = p^{\text{inc}}(x), \\ &\frac{\partial p}{\partial n(x)} = \epsilon p(x). \end{aligned}\right\} \tag{2.37}$$

Hypersingular boundary integral formulation

$$\left.\begin{aligned} &\text{Find } p \text{ such that} \\ &\frac{1}{2}\frac{\partial p}{\partial n(x)}(x) - \oint_\Gamma p(y)\frac{\partial^2 \Phi}{\partial n(x)\,\partial n(y)}(x, y)\,ds(y) \\ &\quad + \int_\Gamma \frac{\partial p}{\partial n(y)}(y)\frac{\partial \Phi}{\partial n(x)}(x, y)\,ds(y) = \frac{\partial p^{\text{inc}}}{\partial n(x)}(x), \\ &\frac{\partial p}{\partial n(x)}(x) = \epsilon p(x). \end{aligned}\right\} \tag{2.38}$$

The calculation of the hypersingular integrals is discussed below.

We conclude this section with the Burton–Miller formulation which is obtained formally by simply taking a linear combination of the Helmholtz formulation and the hypersingular formulation premultiplied by an imaginary factor of i/k where k is the wave number.

Burton–Miller formulation

$$\left.\begin{aligned} &\text{Find } p \text{ such that} \\ &\alpha\left\{\tfrac{1}{2}p(x) - \int_\Gamma p(y)\frac{\partial \Phi}{\partial n(y)}(x, y)\,ds(y) + \int_\Gamma \frac{\partial p}{\partial n(y)}(y)\Phi(x, y)\,ds(y)\right\} \\ &\quad + \frac{(1-\alpha)i}{k}\left\{\frac{1}{2}\frac{\partial p}{\partial n(x)}(x) + \oint_\Gamma p(y)\frac{\partial^2 \Phi}{\partial n(x)\,\partial n(y)}(x, y)\,ds(y) \right. \\ &\qquad \left. + \int_\Gamma \frac{\partial p}{\partial n(y)}(y)\frac{\partial \Phi}{\partial n(x)}(x, y)\,ds(y)\right\} \\ &= \alpha p^{\text{inc}}(x) + \frac{(1-\alpha)i}{k}\frac{\partial p^{\text{inc}}}{\partial n(x)}(x), \\ &\frac{\partial p}{\partial n(x)}(x) = \epsilon p(x), \\ &\alpha \in [0, 1]. \end{aligned}\right\} \tag{2.39}$$

3. Numerical implementation

In what follows, only the Burton–Miller approach will be discussed, since the two previous formulations can be obtained by selecting $\alpha = 1$ or $\alpha = 0$.

Variational formulation

Multiplying both sides of the two equations of (2.39) by a test function $q(x)$ and integrating over Γ, we obtain the following variational formulation:

$$
\begin{aligned}
&\text{Find } p \text{ such that} \\
&\alpha\left\{\frac{1}{2}\int_\Gamma p(x)q(x)\,ds(x) - \int_\Gamma\int_\Gamma p(y)\frac{\partial\Phi}{\partial n(y)}(x,y)\,ds(y)q(x)\,ds(x)\right. \\
&\qquad \left. + \int_\Gamma\int_\Gamma \frac{\partial p}{\partial n(y)}(y)\Phi(x,y)\,ds(y)q(x)\,ds(x)\right\} \\
&\qquad + \frac{(1-\alpha)\mathrm{i}}{k}\left\{\frac{1}{2}\int_\Gamma \frac{\partial p}{\partial n(x)}(x)q(x)\,ds(x)\right. \\
&\qquad\qquad + \int_\Gamma \oint_\Gamma p(y)\frac{\partial^2\Phi}{\partial n(x)\,\partial n(y)}(x,y)\,ds(y)q(x)\,ds(x) \\
&\qquad\qquad \left. + \int_\Gamma\int_\Gamma \frac{\partial p}{\partial n(y)}(y)\frac{\partial\Phi}{\partial n(x)}(x,y)\,ds(y)q(x)\,ds(x)\right\} \\
&= \int_\Gamma\left[\alpha p^{\mathrm{inc}}(x) + \frac{(1-\alpha)\mathrm{i}}{k}\frac{\partial p^{\mathrm{inc}}}{\partial n(x)}(x)\right]q(x)\,ds(x), \\
&\int_\Gamma\left[\frac{\partial p}{\partial n(x)}(x) - \epsilon p(x)\right]ds(x) = 0, \\
&\text{for every } q = q(x).
\end{aligned}
\tag{3.1}
$$

Galerkin approximation

Approximating p, $\partial p/\partial n$ and q with linear combinations of the same basis functions

$$
p(x) = \sum_{k=1}^{N} p^k e_k(x), \qquad \frac{\partial p}{\partial n}(x) = \sum_{k=1}^{N}\left(\frac{\partial p}{\partial n}\right)^k e_k(x), \qquad q(x) = \sum_{k=1}^{N} q^k e_k(x), \tag{3.2}
$$

where $e_k = e_k(x)$ are real-valued basis functions and p^k, $(\partial p/\partial n)^k$, q^k are *complex* coefficients we arrive at a system of (complex) linear equations to be solved for p^k, $(\partial p/\partial n)^k$. (Note that the second equation is *not* interpreted pointwise but only in the weak sense suggesting a type of *mixed* variational formulation.) If $\epsilon = \text{const.}$, the second of equations (3.1) reduces to

$$
\sum_{k=1}^{N}\left[\left(\frac{\partial p}{\partial n}\right)^k - \epsilon p^k\right]\int_\Gamma e_k(x)e_l(x)\,ds(x) = 0, \quad l = 1,\ldots,N, \tag{3.3}
$$

and leads to a direct relation between the degrees of freedom,

$$\left(\frac{\partial p}{\partial n}\right)^k = \epsilon p^k. \tag{3.4}$$

This allows us to eliminate $(\partial p/\partial n)^k$ from the calculations and leads to the final system of equations in the form

$$\sum_{k=1}^{N} a_{kl} p^k = b_l, \quad l-1,\ldots,N, \tag{3.5}$$

where the "load vector" is given by

$$b_l = \int_\Gamma \left[\alpha p^{\text{inc}}(x) + \frac{(1-\alpha)\mathrm{i}}{k}\frac{\partial p^{\text{inc}}}{\partial n(x)}(x)\right] e_l(x)\, ds(x), \tag{3.6}$$

and the stiffness matrix is defined by

$$\begin{aligned} a_{kl} = \alpha\Bigg\{ & \frac{1}{2}\int_\Gamma e_k(y) e_l(x)\, ds(x) - \int_\Gamma\int_\Gamma e_k(y)\frac{\partial \Phi}{\partial n(y)}(x, y)\, ds(y) e_l(x)\, ds(x) \\ & + \epsilon \int_\Gamma\int_\Gamma e_k(y)\Phi(x, y)\, ds(y) e_l(x)\, ds(x)\Bigg\} \\ + \frac{(1-\alpha)\mathrm{i}}{k}\Bigg\{ & \tfrac{1}{2}\epsilon\int_\Gamma e_k(y) e_l(x)\, ds(x) + \int_\Gamma\int_\Gamma e_k(y)\frac{\partial^2 \Phi}{\partial n(x)\,\partial n(y)} \\ & \times(x, y)\, ds(y) e_l(x)\, ds(x) \\ & + \epsilon\int_\Gamma\int_\Gamma e_k(y)\frac{\partial \Phi}{\partial n(x)}(x, y)\, ds(y) e_l(x)\, ds(x)\Bigg\}. \end{aligned} \tag{3.7}$$

h-p approximation

A one-dimensional version of the *h-p* approximation discussed in [6] has been implemented. The principal features of the method are as follows.

- Each element has at most three nodes, two endpoints starting with linear approximation and a middle node for orders of approximation $p \geq 2$ (this spectral order p should not be confused with the pressure). The geometry of the element is defined only by its nodes resulting in a piecewise linear approximation for linear elements and piecewise parabolic for $p \geq 2$.
- Hierarchical shape functions discussed in [28] are implemented.
- The approximation is continuous. The linear degrees of freedom are common for neighboring elements.
- Approximation of geometry (Jacobians, outward normal unit vectors, angles $\beta(x)$, $\beta(y)$, γ) is straightforward. Thus, the approximate boundary is not, in general, C^1-continuous (jumps in normal unit vectors across the interelement nodes).

Most of the implementation (except for the singular integration discussed next) is standard and resembles that for finite elements. Essential differences include a double loop through elements (due to the double integral in the formulation, the element stiffness matrices are defined

for *pairs* of elements) resulting in a fully populated stiffness matrix. A simple, direct Gaussian solver is used to solve the system of algebraic equations.

Singular integration

Let K_1 and K_2 be two elements. A typical contribution to the element stiffness matrix corresponding to K_1 and K_2 is of the form

$$\int_{K_1}\left[\int_{K_2}\chi_k^2(y)\phi(x, y)\,ds(y)\right]\chi_l^1(x)\,ds(x), \tag{3.8}$$

where χ_k^j are shape functions for element K_j, $j=1, 2$. In the case when $K_1 = K_2$, the kernel function $\phi(x, y)$ may be singular. The following numerical procedure for evaluating integrals (3.8) has been implemented.

Case 1: $K_1 \neq K_2$

Both integrals are evaluated using Gaussian integration with the number of integration points $N_l = p+1$ for the outer integral and a simple self-adaptive integration procedure is used for the inner integral. In the adaptive integration, element K_2 is subdivided into 2^n equal subelements and Gaussian quadrature with $N_l = p+1$ integration points is used to calculate the integral. Proceeding with $n = 0, 1, \ldots$, the integration is continued until agreement is obtained between consecutive approximations (up to machine accuracy). By implementing such a simple (and very inefficient) procedure, we merely want at this point to eliminate the effects of approximate integration.

Case 2: $K_1 = K_2$

The outer integral is again evaluated using Gaussian quadrature with $N_l = p+1$ integration points. Integration of the inner integral changes with the type of singularity of the kernel function $\phi(x, y)$ in (3.8). A typical situation is illustrated in Fig. 6. For every Gaussian integration point used to evaluate the outer integral, the integration of the inner integral has to deal with the (possibly) singular behavior of $\phi(x, y)$ at this point. To cope with this, the element is divided into two parts: integrate from one endpoint to the singular point and from the singularity to the other endpoint and the integration is performed separately on each part. Three particular cases are taken into account.

(a) *Regular (bounded) integrand.* For bounded contributions $\phi(x, y)$, each of the two subintegrals is evaluated using Gaussian quadrature with $N_l = p+1$ integration points.

(b) *Weakly singular (logarithmic) integrand.* Each of the two subintegrals is converted into an integral from 0 to d_j, $j=1, 2$, with respect to the *distance* between an integration point and the singular point. A special integration rule for logarithmic kernels of Gaussian type is then used with the number of integration points (too large again) $N_l = p+1$. An additional complication arises due to the lack of an explicit relationship between the integration variable (distance s) and the master element coordinate, say η. This is solved in practice by starting with an initial value for η corresponding to a linear element and performing Newton–Raphson iterations until agreement to machine accuracy is reached. With quadratic elements, the number of iterations is typically equal to 2.

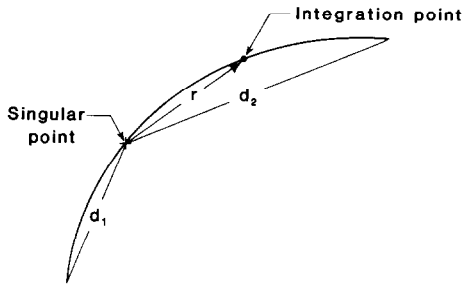

Fig. 6. Evaluation of singular integrals.

(c) *Hypersingular integrand*. The procedure advocated in [8] has been implemented. The inner integral is first converted into an integral with respect to the distance variable (compare Fig. 6)

$$\int_{-d_1}^{d_2} \frac{u(r)}{r^2}\,\mathrm{d}r, \tag{3.9}$$

and then the standard regularization is applied to (3.9) by subtracting from $u(r)$ its first-order Taylor approximation at $r=0$, i.e.,

$$\int_{-d_1}^{d_2} \frac{u(r)}{r^2}\,\mathrm{d}r = \int_{-d_1}^{d_2} \frac{u(r)-u(0)-u'(0)r}{r^2}\,\mathrm{d}r + u(0)\int_{-d_1}^{d_2} \frac{dr}{r^2} + u'(0)\int_{-d_1}^{d_2} \frac{\mathrm{d}r}{r}. \tag{3.10}$$

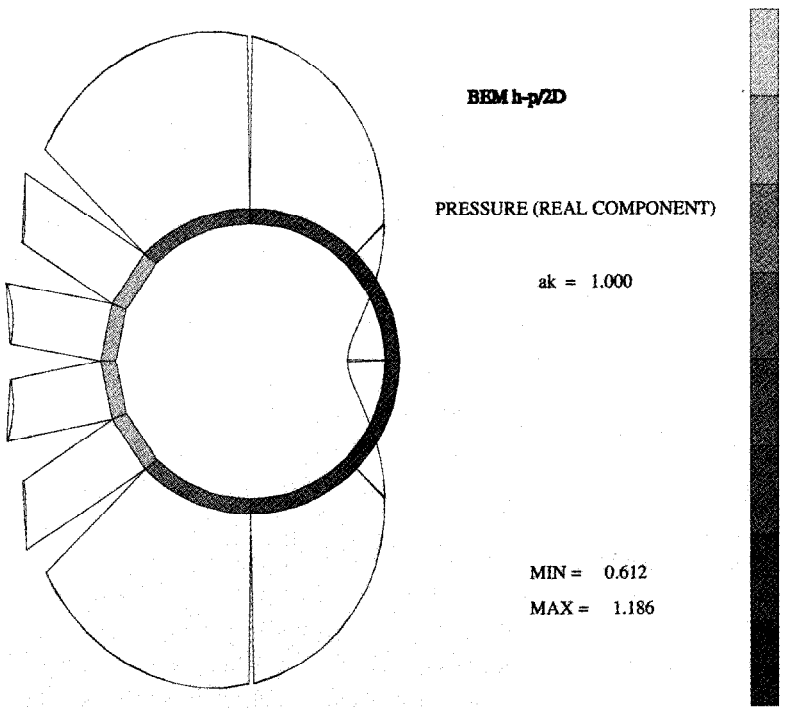

Fig. 7. A typical *h-p* finite-element mesh and a corresponding approximation solution compared with the exact one for the test problem. Different shades indicate different orders of approximation.

The first contribution is then integrated using the Gaussian quadrature (from $-d_1$ to 0 and 0 to d_2 separately) whereas the two remaining integrals are evaluated using the closed forms

$$\int_{-d_1}^{d_2} \frac{\mathrm{d}r}{r^2} = \frac{1}{d_1} - \frac{1}{d_2}, \qquad \int_{-d_1}^{d_2} \frac{\mathrm{d}r}{r} = \ln d_2 - \ln d_1. \tag{3.11}$$

Note that function $u(r)$ in (3.9)–(3.11) incorporates contributions from *both* the shape functions of element K *and* geometrical quantities (Jacobian).

The regularization (3.10) could be performed globally extending the integration over the entire boundary Γ (the singular contribution in such a case would then vanish), but then the algebraic structure of the approximate problem would have changed significantly, at least when compared with the Helmholtz formulation.

We conclude this section with Fig. 7 presenting a typical solution to the test problem of scattering of a plane wave by an elastic cylinder. The finite-element mesh is drawn along the boundary of the cylinder with shades indicating different orders of approximation. The lower line indicates an exact solution discussed in the next section and the other line corresponds to the BI solution.

4. Numerical experiments 1

A test problem

The classical scattering problem (see Fig. 8) for a plane wave impinging on an elastic cylinder (in the sense of our simplified model) of radius a was used to test the method and code. Using the polar coordinates (r, θ), the exact solution to the problem is of the form

$$p = p^{\mathrm{inc}} + p^{\mathrm{s}}, \tag{4.1}$$

where the incident pressure

$$p^{\mathrm{inc}}(r, \theta) = P_{\mathrm{inc}}\, \mathrm{e}^{\mathrm{i}kr\cos\theta}, \tag{4.2}$$

with a constant coefficient P_{inc}, and the scattered pressure p^{s} is evaluated using the series representation

$$p^{\mathrm{s}}(r, \theta) = \sum_{m=0}^{\infty} B_m H_m^{(1)}(kr) \cos(m\theta), \tag{4.3}$$

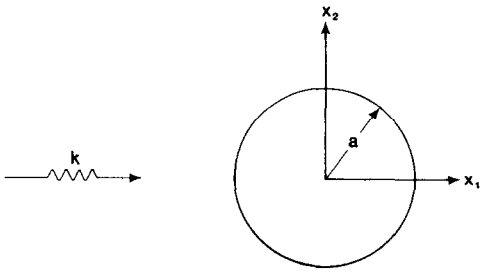

Fig. 8. Scattering of a plane wave by an elastic cylinder. Test problem definition.

with $H_m^{(1)}$ Hankel functions of the first kind of order m and coefficients B_m given by

$$B_m = -P_{\text{inc}}\epsilon_m \mathrm{i}^m \frac{\frac{\mathrm{d}J_m}{\mathrm{d}(kr)}(ka) + \frac{\epsilon}{k}J_m(ka)}{\frac{\mathrm{d}H_m^{(1)}}{\mathrm{d}(kr)}(ka) + \frac{\epsilon}{k}H_m^{(1)}(ka)}, \tag{4.4}$$

where J_m are Bessel functions of the first kind of order m, a is the radius of the cylinder, and

$$\epsilon_m = \begin{cases} 1 & \text{for } m = 0, \\ 2 & \text{for } m = 1, 2, \ldots . \end{cases} \tag{4.5}$$

The constant ϵ was assumed to be a quadratic function of the wavenumber k:

$$\epsilon = \epsilon_0 k^2, \quad \epsilon_0 > 0, \tag{4.6}$$

which is consistent with (1.17). In the case $\epsilon_0 = 0$ the problem reduces to the classical rigid scattering problem.

Rates of convergence

Convergence of the Galerkin method for boundary integral equations have been carefully analyzed in a series of works by Wendland, Stephan et al. [28,29,31]. The main idea is based on an abstract result by Hildebrandt and Wienholtz [9] showing convergence of the Galerkin approximations for (abstract) linear equations of the type

$$Au = f, \tag{4.7}$$

where A is a linear, continuous operator from a Hilbert space X into itself, which can be decomposed into two parts, $A = P + K$, where P is a linear, continuous and positive definite operator from X into itself and K is compact (completely continuous). Frequently we say that A is a compact perturbation of the positive definite operator P.

Identification of the Hilbert space X and operators P and K for a particular boundary integral equation is nontrivial. For instance, for the rigid scattering problems ($\epsilon_0 = 0$) and the hypersingular formulation, X is identified as the fractional Sobolev space $H^{1/2}(\Gamma)$ and an explicit decomposition of A into positive definite and compact parts is difficult to implement in practice (see comments in [31]). The situation is easier for the Helmholtz formulation: X is identified as the space $L^2(\Gamma)$ and P is a scalar multiple of the identity operator (corresponding to the term $\frac{1}{2}p$ on the left-hand side of (2.37)). (No rigorous discussion of the Burton–Miller formulation in a functional analysis setting is known to the authors at this point.)

An additional conclusion arising from the Hildebrandt and Wienholtz [9] result is that the Galerkin procedure is (asymptotically) optimal, i.e., for a given sequence of approximation subspaces $X_h \subset X$, $h \to 0$ and h small enough, the approximation error can be bounded by a product of an h-independent constant c and the distance between the true solution u and the subspace X_h:

$$\| u - u_h \|_X \leqslant c \inf_{v_h \in X_h} \| u - v_h \|_X. \tag{4.8}$$

Here u_h is the approximate solution and $\| \cdot \|_X$ denotes the norm on X. Typically, to obtain an a priori error estimate we substitute for v_h an interpolant of u and express the same fact saying

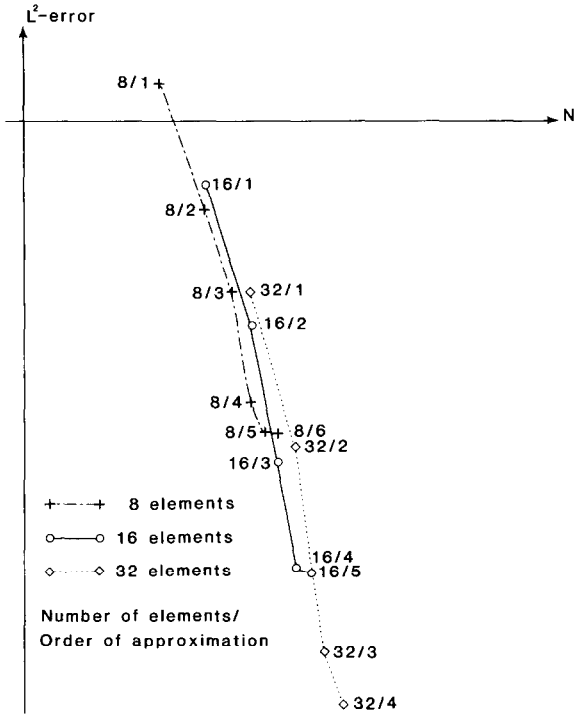

Fig. 9. Example 1. Experimental rates of convergence for uniform p-refinements.

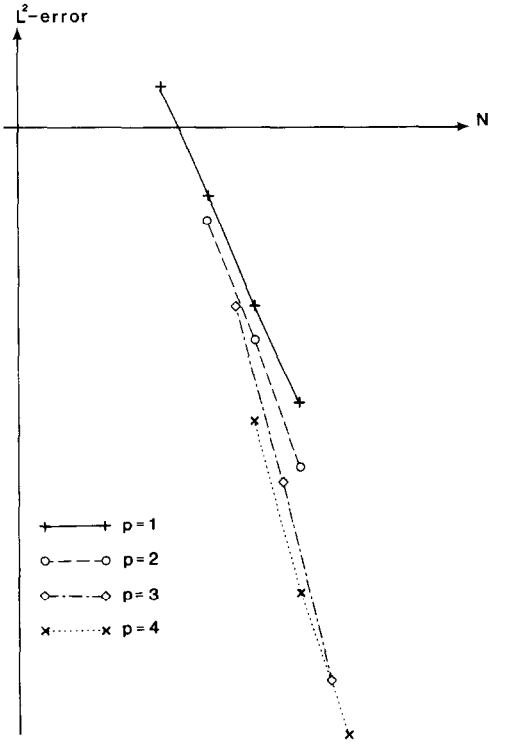

Fig. 10. Example 1. Experimental rates of convergence for uniform h-refinements.

that the approximation error can be bounded by the interpolation error. Thus, whatever the particular rate of convergence that exists for the interpolation error, using h-, p-, h-p, uniform, or adaptive finite elements, exactly the *same* (asymptotic) rate of convergence should be delivered by the Galerkin boundary element method. Using inverse estimates one can show that the interpolation error attains the optimal rate.

The natural (energy) X-norms are the L^2-norm for the Helmholtz formulation and the $H^{1/2}$-norm for the hypersingular case. In our numerical examples, we take the *Aubin–Nitsche* type argument for granted and consider for both formulations only the L^2-norm.

Example 1 (*Rates of convergence for the Helmholtz formulation*). Selecting

$$\epsilon_0 = 0 \quad \text{(rigid scattering)}, \qquad P_{\text{inc}} = 1, \qquad a = 1, \qquad k = 4. \tag{4.9}$$

The test problem was solved using uniform meshes of 8, 16, 32 and 64 elements with order of approximation $p = 1, 2, \ldots, 6$. The corresponding rates of convergence for h-refinements are summarized in Fig. 9 and for the p-refinements in Fig. 10. The rates of convergence for the h-method are very close to the theoretical rate $p + 1$, increasing in particular with the order of approximation p. The rates of convergence for the p-extensions seem to deliver the superlinear (exponential) rate of convergence until the error due to the approximation of the boundary (the exact circle is approximated only with quadratic parabolas) dominates the picture.

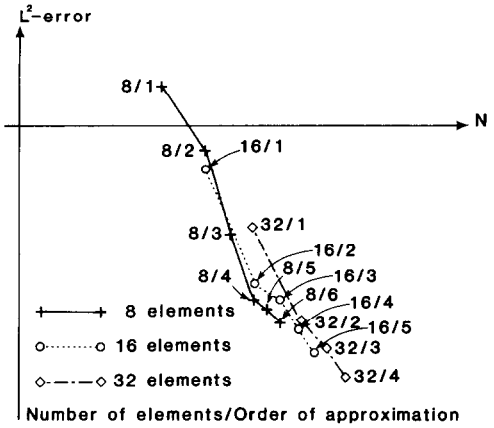

Fig. 11. Example 2. Experimental rates of convergence for uniform p-refinements.

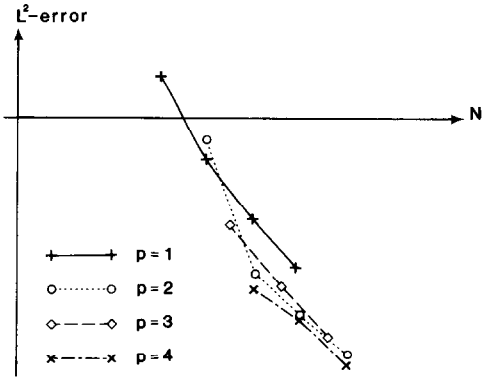

Fig. 12. Example 2. Experimental rates of convergence for uniform h-refinements.

Example 2 (*Rates of convergence for the hypersingular formulation*). With the same data and the same h-p meshes as in the first example, the test problem was solved once again using the hypersingular formulation. The results, summarized in Figs. 11 and 12, are less satisfactory. The observed rates of convergence for the h-method are all close to 1 independent of the order of approximation and the p-method shows no signs of exponential convergence.

The source of these suboptimal rates of convergence is not clear at this writing.

Forbidden frequencies

Restricting our discussion temporarily to only rigid scattering, we recall that the spectrum of the Laplace operator (with Neumann boundary condition) in an exterior domain reduces to its continuous part (no eigenvalues) and, consequently, the exterior Neumann problem for the Helmholtz equation with sufficiently regular data (see, e.g., [1]) always has a unique solution.

In contrast, both boundary integral formulations satisfy only the Fredholm alternative and the nonuniqueness occurs for discrete sets of wave numbers k, frequently called the *forbidden frequencies*. Consequently, for such k, both Helmholtz and hypersingular formulations are *not* equivalent to the original problem and the formulations fail. One can show (see, e.g., [4]) that the forbidden frequencies for the Helmholtz formulation can be identified as the eigenvalues of the corresponding interior Dirichlet problem for the Laplace equation, whereas for the hypersingular formulation they are found to be the eigenvalues of the Neumann problem for the Laplace operator. In particular, the hypersingular formulation will always fail for the limiting static case of $k = 0$.

In [4] Burton and Miller proposed the combination of the two formulations in the form presented in Section 1. The resulting formulation admits a unique solution and is equivalent to the original Helmholtz equation for all wave numbers k.

For another approach to avoid the forbidden frequencies for the Helmholtz formulation, consisting of a modification of the free-space Green's function used in the formulation, see [24].

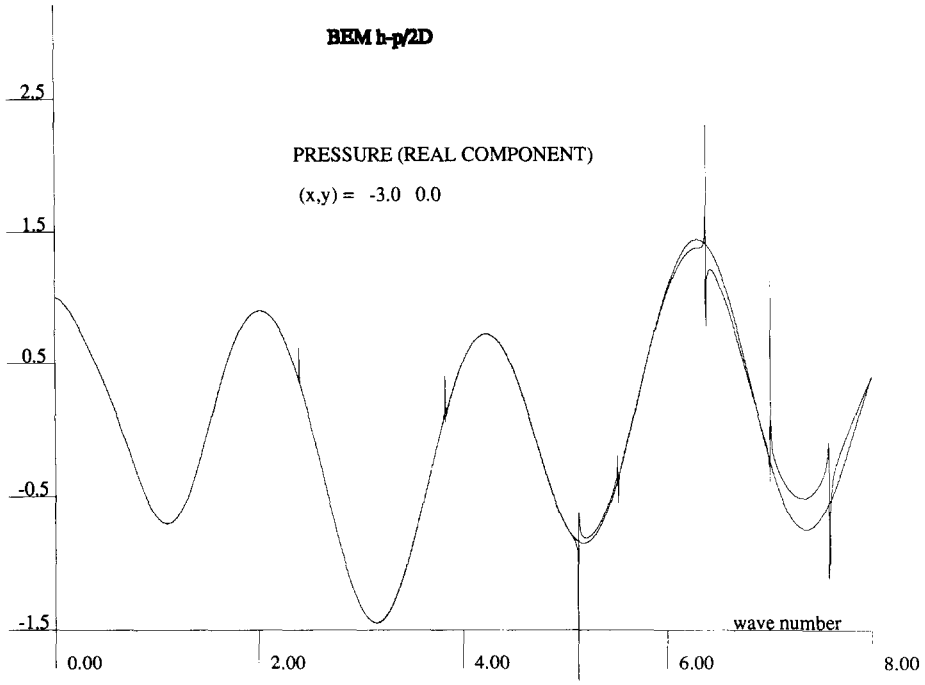

Fig. 13. Example 3. Solution at a field point as a function of wave number for the Helmholtz formulation.

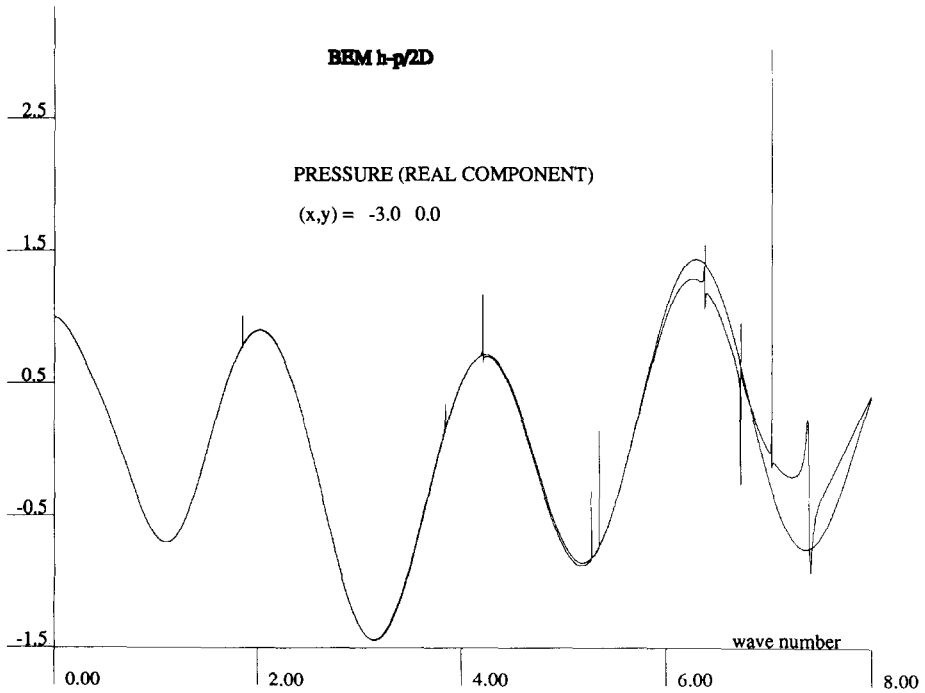

Fig. 14. Example 3. Solution at a field point as a function of wave number for the hypersingular formulation.

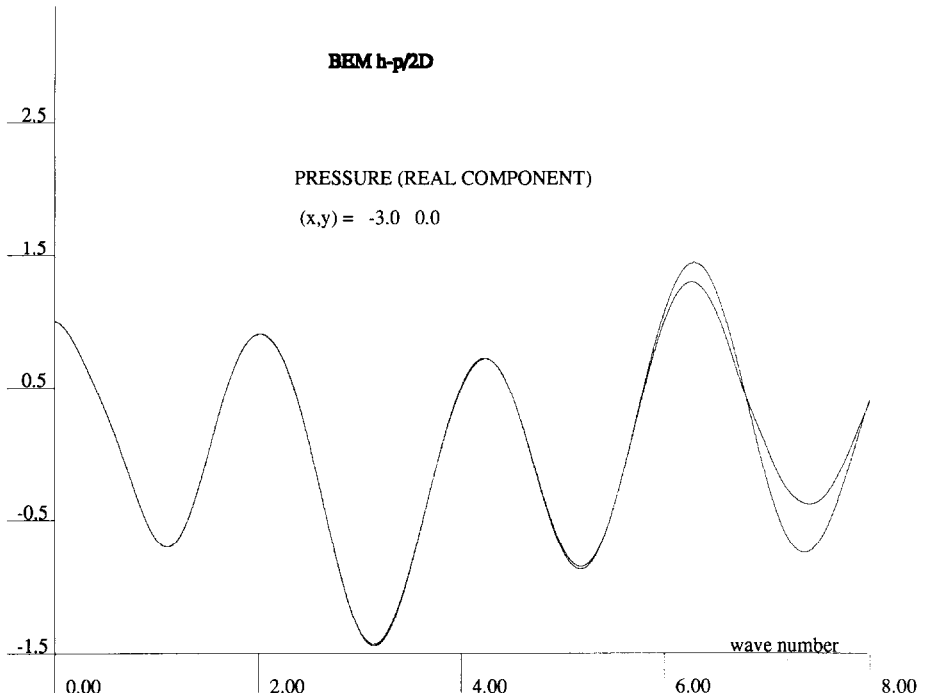

Fig. 15. Example 3. Solution at a field point as a function of wave number for the Burton–Miller formulation.

Example 3 (*Illustration of the forbidden frequencies for the rigid scattering problem*). Theoretically, as long as the wave number k does not coincide *exactly* with a forbidden frequency, the corresponding stiffness matrix is nonsingular and the approximate problem has a unique solution. In practice, for wave numbers k close to the forbidden frequencies, the condition of the matrix deteriorates and the quality of the solution drastically decreases. The situation is illustrated in Figs. 13 and 14 showing the variation of the approximate and exact solutions at a field point $(-3, 0)$ as a function of wave number k. The following data have been chosen:

$$\begin{aligned} &\epsilon_0 = 0 \quad \text{(rigid scattering)}, \qquad P_{\text{inc}} = 1, \\ &a = 1, \qquad \Delta k = 0.002 \quad \text{(increment in wave number)}. \end{aligned} \tag{4.10}$$

For each k, the test problem was solved on the same uniform mesh of 8 quadratic elements. The numerical solution was evaluated using representation formula (2.11) and the approximate solution u_h in place of the exact one. For an element of order p, a $(p+1)$-point Gaussian quadrature rule was used.

Finally, Fig. 15 shows calculations based on the Burton–Miller approach. The method delivers consistently stable results for the whole range of wave numbers k.

Example 4 (*Illustration of the forbidden frequencies for the elastic scattering problem*). Figures 16, 17 and 18 present analogous results for the same test problem as in Example 3, except for the elasticity constant

$$\epsilon_0 = 1. \tag{4.11}$$

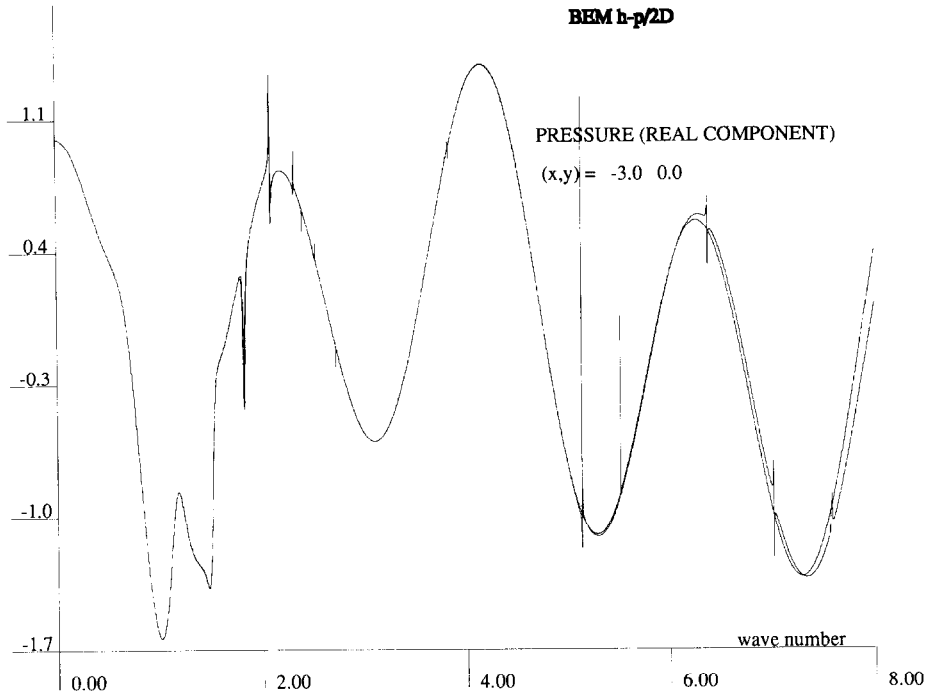

Fig. 16. Example 4. Solution at a field point as a function of wave number for the Helmholtz formulation.

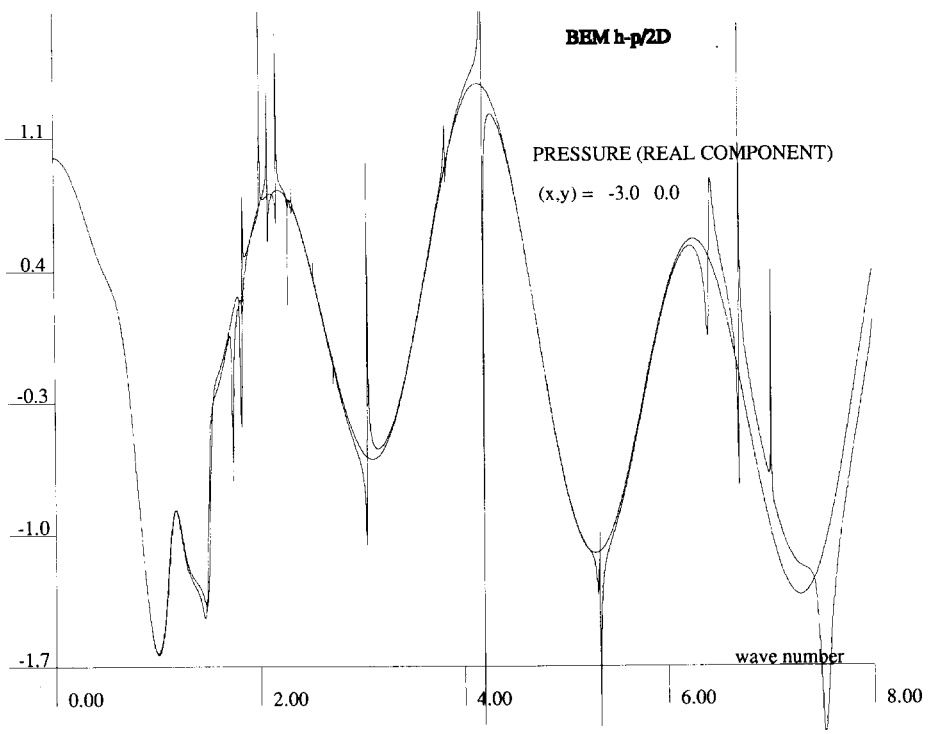

Fig. 17. Example 4. Solution at a field point as a function of wave number for the hypersingular formulation.

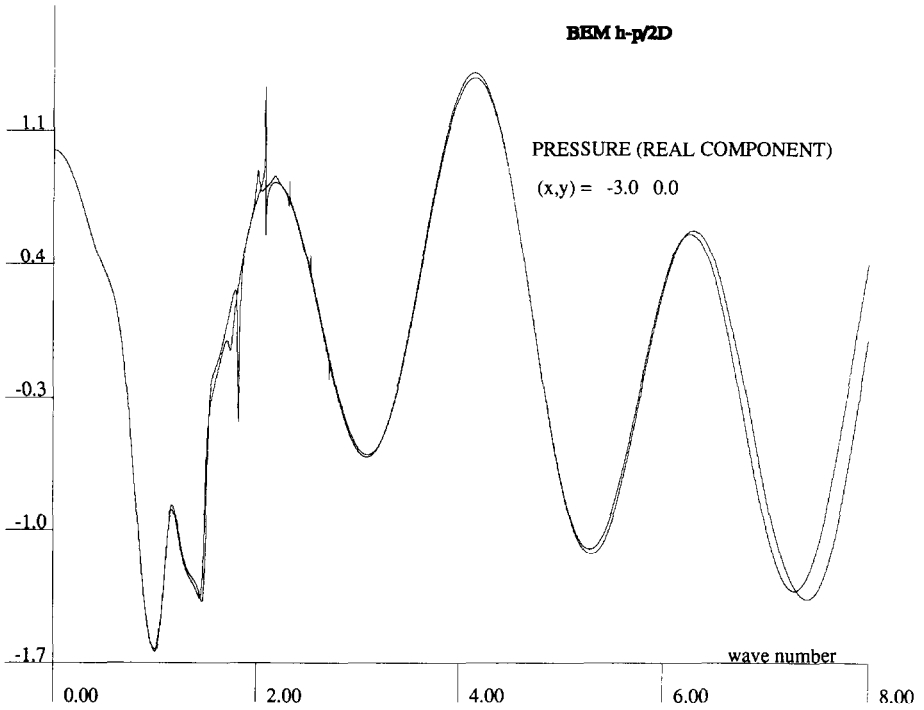

Fig. 18. Example 4. Solution at a field point as a function of wave number for the Burton–Miller formulation.

Notice that this time the original problem experiences some natural frequencies (eigenvalues), closely followed by all three formulations.

5. A posteriori error estimation and adaptivity

In this section we shall restrict ourselves to the rigid scattering case ($\epsilon_0 = 0$).

Helmholtz formulation

Rewriting (2.37) in an operator form typical for integral equations of the second type, we have

$$Ap = (I - 2K)p = 2p^{\text{inc}}, \tag{5.1}$$

where K is the compact operator from $L^2(\Gamma)$ into itself:

$$(Kp)(x) = \int_\Gamma \frac{\partial \Phi}{\partial u(y)}(x, y)p(y)\, ds(y). \tag{5.2}$$

According to the Fredholm alternative for A, if k is not a forbidden frequency, A admits a unique solution for every $p^{\text{inc}} \in L^2(\Gamma)$ and consequently, by the Banach theorem, must be bounded below in $L^2(\Gamma)$, i.e., there exists a constant $c > 0$ such that

$$\| p \|_{L^2(\Gamma)} \leqslant c \| Ap \|_{L^2(\Gamma)}. \tag{5.3}$$

Let u_h denote now *any* approximate solution to (5.1) obtained using some arbitrary method. As long as u_h is an element of $L^2(\Gamma)$, the error $e_h = u - u_h$ satisfies the inequality

$$\| e_h \|_{L^2(\Gamma)} \leqslant c \| 2p^{\text{inc}} - Ap_h \|_{L^2(\Gamma)}. \tag{5.4}$$

The L^2-residual on the right-hand side of (5.4) is a computable quantity and therefore (5.4) can be considered as probably the simplest *global* a posteriori error estimate. Representing it as a sum over all elements

$$\| 2p^{\text{inc}} - Ap_h \|^2_{L^2(\Gamma)} = \sum_K \| 2p^{\text{inc}} - Ap_h \|^2_{L^2(K)}, \tag{5.5}$$

we may use the element contributions, i.e., the element L^2-residuals, as the simplest error indicators. We analyze mathematically this estimate in the next section.

A forbidden frequency case

When k coincides with a forbidden frequency, according to the Fredholm alternative for operator A in (5.1), the corresponding gradient operator $\tilde{A}$ defined on the quotient space $L^2(\Gamma)/\mathcal{N}(A)$ ($\mathcal{N}(A)$ is the finite-dimensional nullspace of A) is still bounded below, i.e.,

$$\| [p] \|_{L^2(\Gamma)/\mathcal{N}(A)} \leqslant c \| Ap \|_{L^2(\Gamma)}, \tag{5.6}$$

or recalling the definition of norm in the quotient space

$$\| [p] \|_{L^2(\Gamma)/\mathcal{N}(A)} = \inf_{q \in \mathcal{N}(A)} \| p - q \|_{L^2(\Gamma)} = \| \Pi p \|_{L^2(\Gamma)}, \tag{5.7}$$

where Π is the L^2-orthogonal projection of p onto the orthogonal complement of $\mathcal{N}(A)$.

Substituting for p the approximation error $p - p_h$, where p_h is again *any* element of $L^2(\Gamma)$, we have

$$\| \Pi e_h \|_{L^2(\Gamma)} \leqslant c \| 2p^{\text{inc}} - Ap_h \|_{L^2(\Gamma)}. \tag{5.8}$$

Thus even in the case when k is a forbidden frequency, the L^2-residual gives an indication of at least a component of the error.

Hypersingular and Burton–Miller formulations

The a posteriori error estimates (5.4) and (5.8) can be used for any element p_h, in particular for p_h resulting from the hypersingular or Burton–Miller formulations. Thus instead of developing a separate error estimation technique based on the hypersingular formulation [32], one can simply use only the Helmholtz formulation for the error estimation, no matter how the approximate solution is obtained.

An adaptive strategy

We conclude this section with a simple adaptive procedure based on the L^2-residual estimate and the equidistribution principle.

Step 1. Select an initial problem
Step 2. Solve the problem
Step 3. Calculate:
- the elements L^2-residuals η_k and the maximum indicator $\eta_{\max} = \max \eta_k$
- the global L^2-residual

$$\eta = \left(\sum_k \eta_k^2 \right)^{1/2} \tag{5.9}$$

- the L^2-norm of the approximate solution p_h, $\| p_h \|$

Step 4. Check the global error:
IF $\eta \leqslant 0.05 \| p_h \|$ THEN
STOP
ELSE
GO TO Step 5
ENDIF
Step 5. Proceed with local refinements
FOR every element K such that $\eta_k \geqslant 0.5\ \eta_{\max}$ refine K
ENDFOR
GO TO Step 2

6. Asymptotic exactness of the a posteriori error estimates

In this section, we establish several mathematical properties of the estimates described in the previous section. In particular, we focus on the problem of obtaining reliable a posteriori error estimates for the Galerkin approximation to the second-kind integral equation: Find $p(\boldsymbol{x}) \in X$ (Hilbert space):

$$p(\boldsymbol{x}) - \int_\Gamma K(\boldsymbol{x}, \boldsymbol{y}) p(\boldsymbol{y})\, \mathrm{d}s(\boldsymbol{y}) = f(\boldsymbol{x}), \quad \boldsymbol{x} \in \Gamma, \tag{6.1}$$

where $K(\boldsymbol{x}, \boldsymbol{y})$ is some known kernel function and $f(\boldsymbol{x})$ is given data on the boundary Γ.

Recall that the Helmholtz formulation (2.37) reduces to the form (6.1) if we assume rigid scattering ($\epsilon_0 = 0$). That is, (2.37) becomes (since $\partial p(\boldsymbol{x})/\partial n(\boldsymbol{x}) = 0$ on Γ):

$$\tfrac{1}{2} p(\boldsymbol{x}) - \int_\Gamma \frac{\partial \Phi(\boldsymbol{x}, \boldsymbol{y})}{\partial \boldsymbol{n}(\boldsymbol{y})} p(\boldsymbol{y})\, \mathrm{d}s(\boldsymbol{y}) = p^{\mathrm{inc}}(\boldsymbol{x}), \quad \boldsymbol{x} \in \Gamma. \tag{6.2}$$

Returning to (6.1), we again assume that the kernel $K(\boldsymbol{x}, \boldsymbol{y})$ determines an operator, which we also denote by $K: X \to X$, which is compact. Moreover, we shall assume that $I - K: X \to X$ is injective. Under these conditions the classical Fredholm alternative may be invoked to deduce the existence of a bounded inverse $(I - K)^{-1}$ and consequently (6.1) has a unique solution. Some remarks were made in the previous section concerning the case of forbidden frequencies which correspond to a nontrivial null space of $I - K$.

We let $(S_n) \subset X$ be any sequence of nested finite-dimensional subspaces of X. That is,

$$S_1 \subset S_2 \subset \cdots \subset S_n \cdots \subset X. \tag{6.3}$$

Such a sequence of subspaces is typically generated by the *h*-, *p*- or *h-p* versions of the boundary element method. The space S_1 is usually composed of low-degree basis functions defined on a relatively coarse partition of Γ serving to model the geometry of the domain. The subspaces S_2, S_3,... are then obtained by enriching the subspace S_1 in various ways:

(1) *h*-refinement — the partitioning of Γ is refined by subdividing elements, either uniformly or by selecting elements on which the error is largest (as indicated by an a posteriori error indicator).

(2) *p*-refinement — the partition of Γ is retained and the subspace S_1 enriched by employing basis functions of increasing degree either uniformly or selectively.

(3) *h-p* refinement — combines the *h*- and *p*-refinement schemes.

In order to maintain maximal overall generality, we shall make only a very general assumption regarding the way in which the subspaces (S_n) are generated amounting to a density assumption:

(D) For any $v \in X$ there exists a sequence $(v_k) \in X$ such that $v_k \in S_k$ and

$$\lim_{k \to \infty} \| v - v_k \|_X = 0. \tag{6.4}$$

Let us remark immediately that (D) will be satisfied for the cases of uniform *h*- or *p*-refinement schemes. The case of adaptive *h-p* refinement, however, will not be covered in general.

The Galerkin approximation p_k from the subspace S_k is defined by:

$$\text{Find } p_k \in S_k: (p_k, v_k) = (f, v_k) + (Kp_k, v_k), \quad \forall v_k \in S_k. \tag{6.5}$$

Introducing the operator $\Pi_k: X \to S_k$ to be the orthogonal projection onto the subspace S_k:

$$(\Pi_k p, v_k) = (p, v_k), \quad \forall v_k \in S_k, \tag{6.6}$$

we may combine (6.1) and (6.5) to obtain the relations

$$p_k = \Pi_k (f + Kp_k) \tag{6.7}$$

and

$$p_k = \Pi_k (p - Kp + Kp_k). \tag{6.8}$$

The residual is defined to be

$$r_k = p_k - Kp_k - f, \tag{6.9}$$

which is readily computable given p_k, since the evaluation of Kp_k employs routines already present in the code used to calculate the approximation p_k itself. The proposed global error estimator is simply taken to be the norm of the residual

$$\eta_k = \| r_k \|_X. \tag{6.10}$$

The local error indicators are taken to be the corresponding element-based quantities

$$\eta_{k,\Omega_\nu} = \| r_k \|_{X,\Omega_\nu}. \tag{6.11}$$

Supposing that the norm on X is additive, we obtain

$$\eta_k = \left(\sum_{\Omega_\nu} \eta_{k,\Omega_\nu}^2 \right)^{1/2}. \tag{6.12}$$

For our applications, the norm will be the L^2-norm on the boundary which is readily seen to be additive.

Residual type error estimators similar to (6.12) have been proposed and used by several authors (see [20,32,33]). In the latter references the estimators are shown to be equivalent to the discretization error, i.e., there exist numbers c_1 and c_2 such that

$$c_1 \| r_k \|_X \leqslant \| e_k \|_X = \| p - p_k \|_X \leqslant c_2 \| r_k \|_X. \tag{6.13}$$

However, c_1 depends upon the maximum mesh spacing h and $c_1 \to 0$ as $h \to 0$. Also, (6.13) is subject to rather strong assumptions which have been verified only in the case of piecewise constant and piecewise linear approximation schemes on uniform meshes (see [32, Assumptions 1, 2]). Finally, the numbers c_1 and c_2 are not known explicitly and consequently lead to difficulties in using (6.13) as the basis of a stopping criterion for adaptive analysis. The analysis which we shall present is much simpler than in [32] and requires only the assumptions made hitherto. However, problems arising from the nonlocal nature of the operator K are not discussed.

Lemma 6.1. *Suppose $K: X \to X$ is compact and $(I - K): X \to X$ is injective; then there exist constants c_1 and c_2 which are independent of (S_k) such that*

$$c_1 \eta_k \leqslant \| e_k \|_X \leqslant c_2 \eta_k. \tag{6.14}$$

Proof. Observe from (6.9) and (6.1) that

$$r_k = p_k - Kp_k - f = p_k - Kp_k - p + Kp = -(I - K)e_k, \tag{6.15}$$

so that, since K is compact and therefore bounded,

$$\| r_k \|_X \leqslant \| I - K \| \cdot \| e_k \|_X,$$

and the left-hand inequality holds with $c_1 = \| I - K \|^{-1}$. Since $I - K$ is injective, by the Fredholm alternative, $(I - K)^{-1}: X \to X$ exists and is bounded. Therefore from (6.15) we obtain

$$\| e_k \|_X \leqslant \| (I - K)^{-1} \| \cdot \| r_k \|_X,$$

and the right-hand inequality holds with $c_2 = \| (I - K)^{-1} \|$. □

The result of Lemma 6.1 is well known and was also shown in [32]. In the following, we work toward a stronger result which shows that the effectivity index θ_k, under assumption (6.4),

$$\theta_k = \frac{\eta_k}{\| e_k \|} \to 1 \quad \text{as } k \to \infty. \tag{6.16}$$

This property is known as *asymptotic exactness*. In terms of practical computation, it means that we may use η_k as a stopping criterion for the adaptive algorithm and that η_k gives realistic estimates of the error. The key step in the analysis is to interpret the residual estimation technique in terms of a recovery-based estimation technique (see [2]). This interpretation then allows one to demonstrate asymptotic exactness.

The iterated Galerkin technique [26,27] is a postprocessing technique used for improving the Galerkin approximation to solutions of second-kind integral equations. The first iterate is defined by

$$\tilde{p}_k = f + Kp_k, \tag{6.17}$$

where $p_k \in S_k$ is the Galerkin approximation.

Lemma 6.2. *Suppose* (D) *holds,* $K: X \to X$ *is compact and* $(I-K): X \to X$ *is injective; then for* k *sufficiently large we have*

$$\|p-\tilde{p}_k\|_X \leqslant \mu(k)\,\|p-p_k\|_X, \tag{6.18}$$

where $\mu(k) \to 0$ *as* $k \to \infty$.

Proof. Under the hypotheses it may be shown (see, e.g., [17]) that $(I-K\Pi_k)^{-1}$ exists and is bounded. Moreover, from (6.17) and (6.1)

$$(I-K\Pi_k)(p-\tilde{p}_k) = p-\tilde{p}_k - K\Pi_k p + K\Pi_k \tilde{p}_k = K(p-p_k) - K\Pi_k(p-\tilde{p}_k).$$

Further, from (6.17)

$$\Pi_k(p-\tilde{p}_k) = \Pi_k(p-f-Kp_k) = \Pi_k p - \Pi_k f + \Pi_k K p_k = \Pi_k p - \Pi_k p_k \quad \text{from (6.7)}$$
$$= \Pi_k e_k.$$

Therefore,

$$(I-K\Pi_k)(p-\tilde{p}_k) = (K-K\Pi_k)e_k,$$

and hence

$$\|p-\tilde{p}_k\|_X \leqslant \mu(k)\,\|e_k\|_X,$$

where

$$\mu(k) = \left\|(I-K\Pi_k)^{-1}\right\| \cdot \|K\| \cdot \|I-\Pi_k\|.$$

The result follows since by (D),

$$\|I-\Pi_k\| = \sup_{\substack{v\in X \\ \|v\|_X=1}} \|v-\Pi_k v\|_X \to 0 \quad \text{as } k \to \infty. \qquad \square$$

Our main result is as follows.

Theorem 6.3. *Suppose* (D) *holds,* $K: X \to X$ *is compact and* $(I-K): X \to X$ *is injective; then*

$$\lim_{k\to\infty} \theta_k = 1, \tag{6.19}$$

where $\theta_k = \eta_k / \|e_k\|_X$ *is the effectivity index.*

Proof.

$$\eta_k = \|r_k\|_X = \|p_k - (f+Kp_k)\|_X = \|p_k - \tilde{p}_k\|_X \quad \text{from (6.17)}$$
$$\leqslant \|p_k - p\|_X + \|p-\tilde{p}_k\|_X \leqslant \{1+\mu(k)\}\,\|p-p_k\|_X \quad \text{by Lemma 6.2.}$$

Furthermore,

$$\|e_k\|_X \leqslant \|p-\tilde{p}_k\|_X + \|\tilde{p}_k - p_k\| \leqslant \mu(k)\,\|e_k\|_X + \|\tilde{p}_k - p_k\|_X \quad \text{by Lemma 6.2.}$$

Hence for sufficiently large k

$$1-\mu(k) \leqslant \theta_k \leqslant 1+\mu(k),$$

and by Lemma 6.2 we have

$$\lim_{k\to\infty} \theta_k = 1. \qquad \square$$

7. Numerical experiments 2

Example 5 (*Global effectivity of the L^2-residual estimate*). We begin with a simple comparison of the L^2-error and L^2-residual for the test problem with data and meshes discussed in Examples 1 and 2. Table 1 summarizes results for the Helmholtz formulation and Table 2 for the hypersingular formulation. The following conclusions can be drawn.

- For the Helmholtz formulation the L^2-residual seems to give an asymptotically exact error estimate for the h-refinements, as predicted by Theorem 6.3.
- For the p-refinements and the Helmholtz formulation, the effectivity index decreases for large p, supposedly because of the domination of the error due to the geometry approximation (*not* taken into account in the discussion in the previous section).
- For the hypersingular formulation, the global effectivity index stays bounded but, as expected, does not converge to 1.

Example 6 (*Local effectivity of the L^2-residual estimates*). With the same data as in Example 5, Table 3 presents the comparison of local L^2-errors and L^2-residuals for a mesh of 8 quadratic elements and Helmholtz and hypersingular formulations. In both cases the local effectivity indices stay very close to the corresponding global ones indicating the rationality of using the local L^2-residuals as a basis for refinements.

Example 7 (*Global effectivity of the L^2-residual estimate for a forbidden frequency*). Table 4 presents the results of the error estimation for the test problem for the first forbidden frequency

Table 1
Example 5. Comparison of global L^2-errors with L^2-residuals for the Helmholtz formulation

Number of elements	p	L^2-error squared	L^2-residual squared	Global effectivity index
8	1	3.214	2.173	0.82
8	2	$6.708 \cdot 10^{-2}$	$6.782 \cdot 10^{-2}$	1.01
8	3	$5.838 \cdot 10^{-3}$	$5.934 \cdot 10^{-3}$	1.01
8	4	$1.743 \cdot 10^{-4}$	$1.279 \cdot 10^{-4}$	0.85
8	5	$7.152 \cdot 10^{-5}$	$8.323 \cdot 10^{-6}$	0.34
8	6	$7.096 \cdot 10^{-5}$	$3.878 \cdot 10^{-6}$	0.23
16	1	0.144	0.143	1.00
16	2	$2.009 \cdot 10^{-3}$	$2.038 \cdot 10^{-3}$	1.01
16	3	$2.819 \cdot 10^{-5}$	$2.769 \cdot 10^{-5}$	0.99
16	4	$1.222 \cdot 10^{-6}$	$1.753 \cdot 10^{-7}$	0.38
16	5	$1.147 \cdot 10^{-6}$	$6.187 \cdot 10^{-8}$	
32	1	$5.835 \cdot 10^{-3}$	$5.761 \cdot 10^{-3}$	0.99
32	2	$5.284 \cdot 10^{-5}$	$5.329 \cdot 10^{-5}$	1.00
32	3	$9.423 \cdot 10^{-8}$	$78.192 \cdot 10^{-8}$	0.87
32	4	$1.984 \cdot 10^{-8}$	$5.317 \cdot 10^{-10}$	0.05
64	1	$3.245 \cdot 10^{-4}$	$2.972 \cdot 10^{-4}$	0.96
64	2	$1.006 \cdot 10^{-6}$	$1.010 \cdot 10^{-6}$	1.00

Table 2
Example 5. Comparison of global L^2-errors with L^2-residuals for the hypersingular formulation

Number of elements	p	L^2-error squared	L^2-residual squared	Global effectivity index
8	1	3.218	4.512	1.18
8	2	0.489	1.439	1.71
8	3	$4.114 \cdot 10^{-2}$	0.129	1.77
8	4	$6.001 \cdot 10^{-3}$	$1.716 \cdot 10^{-2}$	1.69
8	5	$4.495 \cdot 10^{-3}$	$1.521 \cdot 10^{-2}$	1.84
8	6	$2.837 \cdot 10^{-3}$	$9.732 \cdot 10^{-3}$	1.85
16	1	0.294	0.600	1.43
16	2	$9.336 \cdot 10^{-3}$	$2.722 \cdot 10^{-2}$	1.71
16	3	$6.206 \cdot 10^{-3}$	$2.054 \cdot 10^{-2}$	1.82
16	4	$2.507 \cdot 10^{-3}$	$8.591 \cdot 10^{-3}$	1.85
16	5	$1.270 \cdot 10^{-3}$	$4.371 \cdot 10^{-3}$	1.85
32	1	$5.040 \cdot 10^{-2}$	0.118	1.53
32	2	$3.004 \cdot 10^{-3}$	$1.063 \cdot 10^{-2}$	1.88
32	3	$1.454 \cdot 10^{-3}$	$4.970 \cdot 10^{-3}$	1.85
32	4	$6.338 \cdot 10^{-4}$	$2.184 \cdot 10^{-3}$	1.86
64	1	$1.140 \cdot 10^{-2}$	$2.720 \cdot 10^{-2}$	1.55
64	2	$9.176 \cdot 10^{-4}$	$3.207 \cdot 10^{-3}$	1.87

Table 3
Example 6. Comparison of local L^2-errors and L^2-residuals for a mesh of 8 quadratic elements and both the Helmholtz and hypersingular formulations

Element Number	Helmholtz formulation			Hypersingular formulation		
	L^2-error	L^2-residual	Effectivity index	L^2-error	L^2-residual	Effectivity index
1	$2.303 \cdot 10^{-2}$	$2.383 \cdot 10^{-3}$	1.02	$3.640 \cdot 10^{-2}$	0.128	1.87
2	$1.156 \cdot 10^{-2}$	$1.178 \cdot 10^{-2}$	1.01	$7.405 \cdot 10^{-2}$	0.216	1.71
3	$1.382 \cdot 10^{-2}$	$1.396 \cdot 10^{-2}$	1.01	$5.984 \cdot 10^{-2}$	0.183	1.75
4	$5.845 \cdot 10^{-2}$	$5.781 \cdot 10^{-2}$	0.99	$7.438 \cdot 10^{-2}$	0.191	1.60
Global quantities						
	$6.708 \cdot 10^{-2}$	$6.782 \cdot 10^{-2}$	1.01	0.489	1.439	1.71

Table 4
Example 7. Comparison of global L^2-error and L^2-residual for the hypersingular formulation and $k = 2.4048$ (the first forbidden frequency for the Helmholtz formulation) on a sequence of meshes of quadratic elements

Number of elements	L^2-error squared	L^2-residual squared	Effectivity index
8	$1.295 \cdot 10^{-2}$	$1.711 \cdot 10^{-2}$	1.15
16	$9.563 \cdot 10^{-4}$	$2.441 \cdot 10^{-3}$	1.60
32	$2.587 \cdot 10^{-4}$	$7.005 \cdot 10^{-4}$	1.64
64	$7.405 \cdot 10^{-5}$	$1.918 \cdot 10^{-4}$	1.61

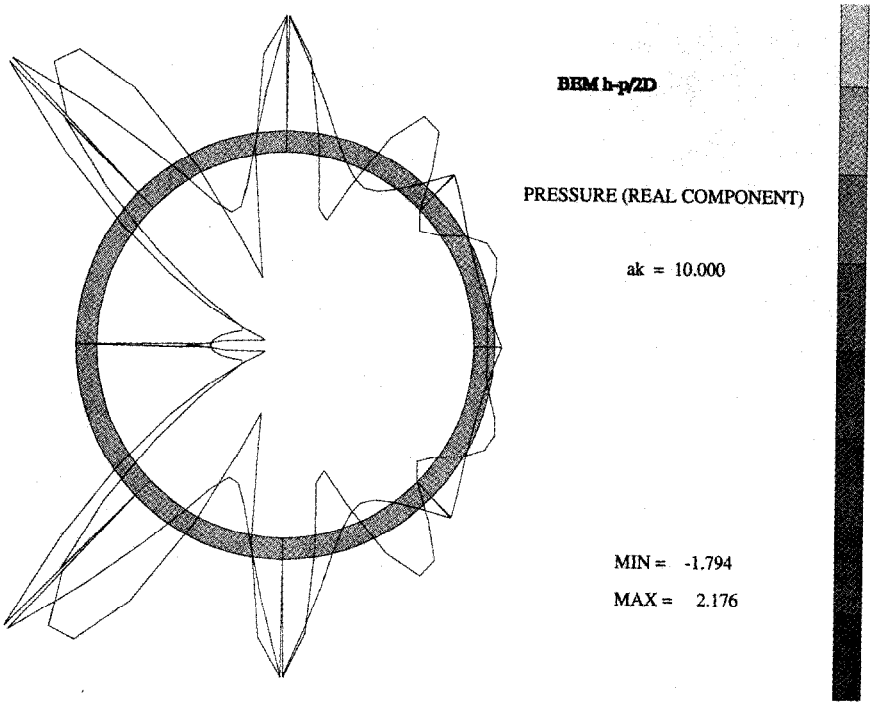

Fig. 19. Example 8. Initial approximate solution on a mesh of 8 quadratic elements.

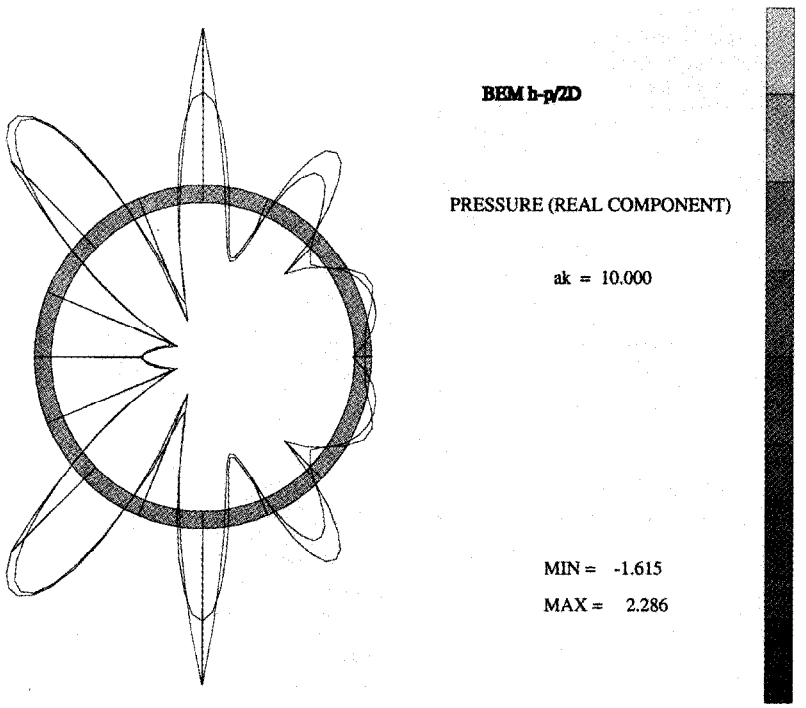

Fig. 20. Example 8. An intermediate, self-adaptive approximate solution.

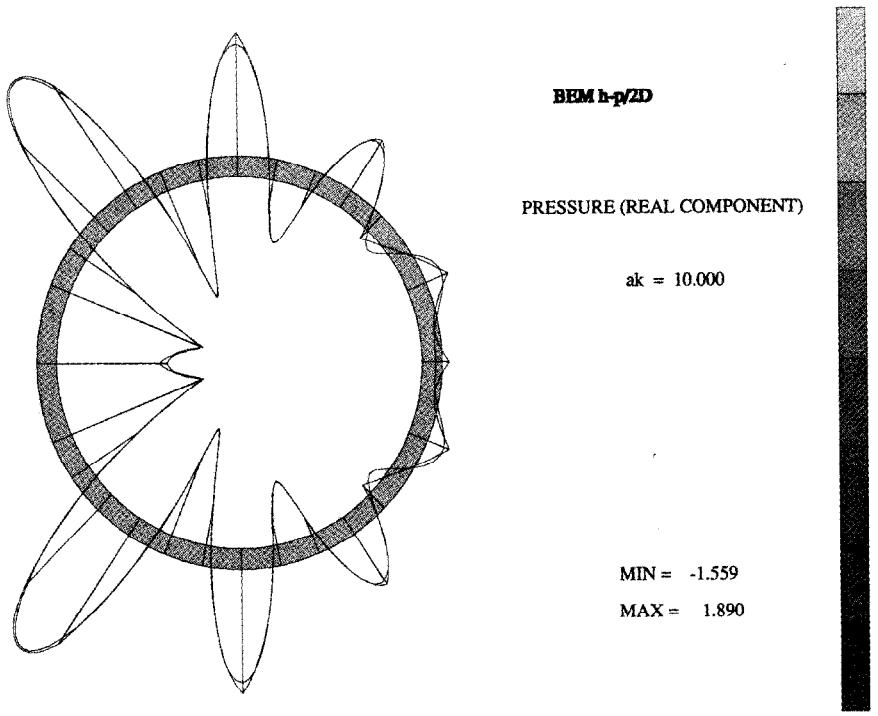

Fig. 21. Example 8. Final adaptive mesh and corresponding approximate solution compared with the exact one.

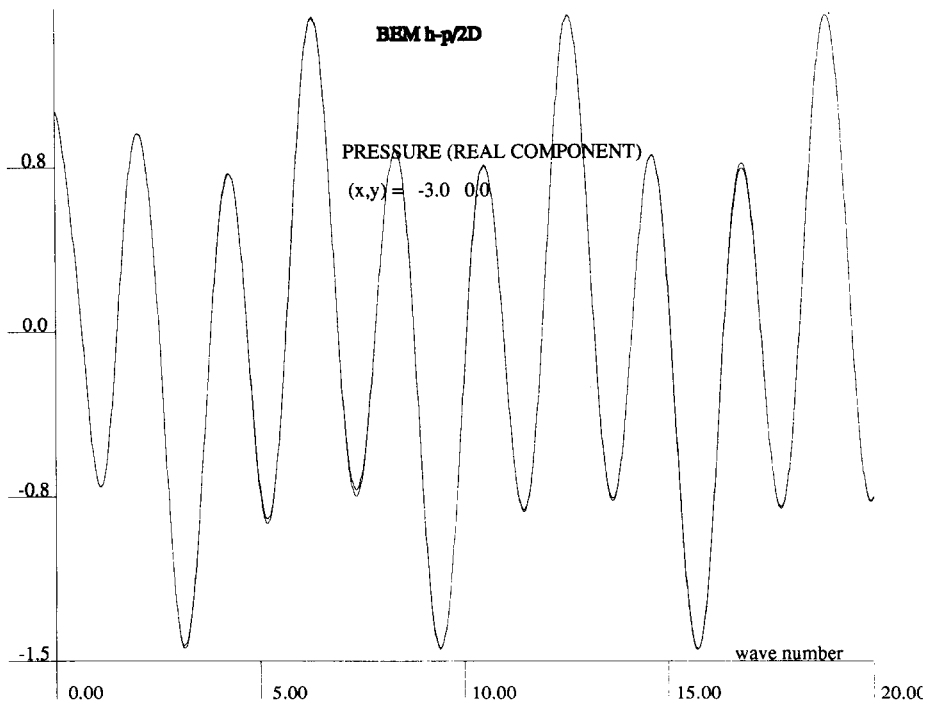

Fig. 22. Example 8. Solution at a field point using adaptive boundary elements as a function of wave number.

for the Helmholtz formulation (the first root of the Bessel function of the first kind and order zero, $k \simeq 2.408$), obtained using hypersingular formulation. The displayed values of the global effectivity indices stay consistently in the same range as in Table 2, indicating that the L^2-residual corresponding to the Helmholtz formulation can be used for the entire range of frequencies, provided the $\mathcal{N}(A)$-component of the error is eliminated by an appropriate (in this case hypersingular) formulation.

Example 8 (*Example of an adaptive solution*). As an illustration for the adaptive procedure discussed in the previous section, we present a p-adaptive solution to the test problem with data

$$\epsilon_0 = 0, \qquad a = 1, \qquad P_{\text{inc}} = 1, \qquad k = 20. \tag{7.1}$$

Figures 19, 20 and 21 present the initial, intermediate, and final solution with the error less than 5 percent of the L^2-norm of the solution. Finally, Fig. 22 presents the comparison of the exact and adaptive, approximate solutions in the wave number range from 0 to 20 using the Burton–Miller formulation.

Acknowledgements

We would like to thank L. Schuetz, M. Stern and F. Rizzo for interesting and invaluable discussions.

References

[1] J.F. Ahner and R.E. Kleinman, The exterior Neumann problem for the Helmholtz equation, *Arch. Rational Mech. Anal.* **52** (1973) 26–43.

[2] M. Ainsworth and A.W. Craig, Superconvergence and a posteriori error estimation in the finite element method, submitted.

[3] I. Babuška, B.Q. Guo and E.P. Stephan, On the exponential convergence of the *h-p* version for boundary element Galerkin methods on polygons, *Math. Methods Appl. Sci.* **12** (1990) 413–427.

[4] A.J. Burton and G.F. Miller, The application of integral equation methods to the numerical solution of some exterior boundary-value problems, *Proc. Roy. Soc. London Ser. A* **323** (1971) 201–210.

[5] M. Costabel and E.P. Stephan, Boundary integral equations for mixed boundary value problems in polygonal domains and Galerkin approximations, in: W. Fiszdon and K. Wilmański, Eds., *Mathematical Models and Methods in Mechanics*, Banach Center Publ. **15** (PWN, Warsaw, 1985) 175–251.

[6] L. Demkowicz, J.T. Oden, W. Rachowicz and O. Hardy, Toward a universal *h-p* adaptive finite element strategy, Part 1. Constrained approximation and data structure, *Comput. Methods Appl. Mech. Engrg.* **77** (1–2) (1989) 79–112.

[7] G.C. Everstine, M.F. Henderson and L.S. Schuetz, Coupled finite element/boundary element approach for acoustic radiation and scattering, preprint, 1989.

[8] M. Guiggiani, G. Kirshnasamy, T.J. Rudolphi and F.J. Rizzo, A general algorithm for the numerical solution of hypersingular boundary integral equations, preprint, 1990; *J. Appl. Mech.*, submitted.

[9] S. Hildebrandt and E. Wienholtz, Constructive proofs of representation theorems in separable Hilbert space, *Comm. Pure Appl. Math.* **XVII** (1964) 369–373.

[10] G.C. Hsiao and W.L. Wendland, A finite element method for some integral equations of the first kind, *J. Math. Anal. Appl.* **58** (1977) 449–481.

[11] D.S. Jones, Integral equations for the exterior acoustic problem, *Quart. J. Mech. Appl. Math.* **27** (1974) 129–142.

[12] M.C. Junger, Approaches to acoustic fluid-elastic structure interactions, *J. Acoust. Soc. Amer.* **82** (4) (1987) 1115–1121.
[13] M.C. Junger and D. Feit, *Sound, Structures and Their Interaction* (MIT Press, Cambridge, MA, 2nd ed., 1986).
[14] G. Kirshnasamy, L.W. Schmerz, T.J. Rudolphi and F.J. Rizzo, Hypersingular boundary integral equations: some applications in acoustics and elastic wave scattering, *J. Appl. Mech.*, to appear.
[15] R.E. Kleinman, G.F. Roach, L.S. Schuetz and J. Shirron, An iterative solution to acoustic scattering by rigid objects, *J. Acoust. Soc. Amer.* **84** (1) (1988) 385–391.
[16] R.E. Kleinman and W.L. Wendland, On Neumann's method for the exterior Neumann problem for the Helmholtz equation, *J. Math. Anal. Appl.* **57** (1977) 170–202.
[17] R. Kress, *Linear Integral Equations*, Appl. Math. Sci. **82** (Springer, Berlin, 1989).
[18] R. Leis, *Initial Boundary Value Problems in Mathematical Physics* (Wiley, New York, 1986).
[19] P.A. Martin, F.J. Rizzo and I.R. Gonsales, On hypersingular boundary integral equations for certain problems in mechanics, *Mech. Res. Comm.* **16** (2) (1989) 65–71.
[20] E. Rank, Adaptive *h*-, *p*-, and *hp*-versions for boundary integral element methods, *Internat. J. Numer. Methods Engrg.* **28** (1989) 1335–1349.
[21] J.J. Rencis and K.-Y. Jong, Error estimation for boundary element analysis, *ASCE J. Engrg. Mech.* **115** (9) (1989) 1993–2010.
[22] J.J. Rencis and K.-Y. Jong, A self-adaptive *h*-refinement technique for the boundary element method, *Comput. Methods Appl. Mech. Engrg.* **73** (3) (1989) 295–316.
[23] J.J. Rencis and R.L. Mullen, A self-adaptive mesh refinement technique for boundary element solution of the Laplace equation, *Comput. Mech.* **3** (1988) 309–319.
[24] G.F. Roach, Boundary integral equations and modified Green's functions, in: B. Bojarski and R. Owilewicz, Eds., *Partial Differential Equations*, Banach Center Publ. **19** (PWN, Warsaw, 1987) 237–261.
[25] A.F. Seybert, B. Soenarko, F.J. Rizzo and D.J. Shippy, An advanced computational method for radiation and scattering of acoustic waves in three dimensions, *J. Acoust. Soc. Amer.* **77** (2) (1985) 362–368.
[26] I.H. Sloan, Improvements by iteration for compact operator equations, *Math. Comp.* **30** (1976) 758–764.
[27] I.H. Sloan and V. Thomée, Superconvergence of the Galerkin iterates for integral equations of the second kind, *J. Integral Equations* **9** (1985) 1–23.
[28] E.P. Stephan and M. Suri, On the convergence of the *p*-version of the boundary element Galerkin method, *Math. Comp.* **52** (1989) 31–48.
[29] E.P. Stephan and M. Suri, An *h-p* method with quasiuniform mesh for integral equations on polygons, preprint, 1989.
[30] F. Ursell, On the exterior problems of acoustics: II, *Math. Proc. Cambridge Philos. Soc.* **84** (1978) 545–548.
[31] W.L. Wendland, Asymptotic accuracy and convergence, in: C. Brebbia, Ed., *Progress in Boundary Element Methods* (Academic Press, New York, 1981).
[32] W.L. Wendland and D.H. Yu, Adaptive boundary element methods for strongly elliptic integral equations, *Numer. Math.* **53** (1988) 539–558.
[33] D. Yu, A posteriori error estimates and adaptive approaches for some boundary element methods, in: C.A. Brebbia, W.L. Wendland and G. Kuhn, Eds., *Boundary Element Methods, IX, Vol. 1* (Springer, Berlin, 1987) 241–256.